

# Radiative corrections to the semileptonic and hadronic Higgs-boson decays $H \rightarrow WW/ZZ \rightarrow 4 \text{ fermions}$

A. BREDENSTEIN<sup>1</sup>, A. DENNER<sup>2</sup>, S. DITTMAYER<sup>3</sup> AND M.M. WEBER<sup>4</sup>

<sup>1</sup> *High Energy Accelerator Research Organization (KEK),  
Tsukuba, Ibaraki 305-0801, Japan*

<sup>2</sup> *Paul Scherrer Institut, Würenlingen und Villigen,  
CH-5232 Villigen PSI, Switzerland*

<sup>3</sup> *Max-Planck-Institut für Physik (Werner-Heisenberg-Institut),  
D-80805 München, Germany*

<sup>4</sup> *Fachbereich Physik, Bergische Universität Wuppertal,  
D-42097 Wuppertal, Germany*

**Abstract:**

The radiative corrections of the strong and electroweak interactions are calculated for the Higgs-boson decays  $H \rightarrow WW/ZZ \rightarrow 4f$  with semileptonic or hadronic four-fermion final states in next-to-leading order. This calculation is improved by higher-order corrections originating from heavy-Higgs-boson effects and photonic final-state radiation off charged leptons. The W- and Z-boson resonances are treated within the complex-mass scheme, i.e. without any resonance expansion or on-shell approximation. The calculation essentially follows our previous study of purely leptonic final states. The electroweak corrections are similar for all four-fermion final states; for integrated quantities they amount to some per cent and increase with growing Higgs-boson mass  $M_H$ , reaching 7–8% at  $M_H \sim 500 \text{ GeV}$ . For distributions, the corrections are somewhat larger and, in general, distort the shapes. Among the QCD corrections, which include corrections to interference contributions of the Born diagrams, only the corrections to the squared Born diagrams turn out to be relevant. These contributions can be attributed to the gauge-boson decays, i.e. they approximately amount to  $\alpha_s/\pi$  for semileptonic final states and  $2\alpha_s/\pi$  for hadronic final states. The discussed corrections have been implemented in the Monte Carlo event generator PROPHECY4F.<sup>†</sup>

November 2006

---

<sup>†</sup>The computer code can be obtained from the authors upon request.

## 1 Introduction

The startup of the Large Hadron Collider (LHC) in 2007 will open up a new era in particle physics. One of the main tasks of the LHC will be the detection and the study of the Higgs boson. If it is heavier than 140 GeV and behaves as predicted by the Standard Model (SM), it decays predominantly into gauge-boson pairs and subsequently into four light fermions. From a Higgs-boson mass  $M_H$  of about 130 GeV up to the Z-boson-pair threshold  $2M_Z$ , the decay signature  $H \rightarrow WW^* \rightarrow 2 \text{ leptons} + \text{missing } p_T$  [1] has the highest discovery potential for the Higgs boson at the LHC [2]. For higher Higgs-boson masses, the leading role is taken over by the “gold-plated” channel  $H \rightarrow ZZ \rightarrow 4 \text{ leptons}$ , which will allow for the most accurate measurement of  $M_H$  above 130 GeV [3]. More details and recent developments concerning Higgs-boson studies at the LHC can be found in the literature [4, 5]. At a future  $e^+e^-$  linear collider [6], the decays  $H \rightarrow 4f$  will enable measurements of the  $H \rightarrow WW/ZZ$  branching ratios at the level of a few to 10% [7].

At the LHC, owing to the huge background of strongly interacting particles, the most important decay modes in  $H \rightarrow WW/ZZ \rightarrow 4f$  are those with leptons in the final state. Therefore, most analyses are based on them. However, also final states involving quarks can be useful owing to their larger branching fractions. For decays involving intermediate W bosons these provide better kinematical information since they involve less neutrinos. For instance, it has been found that in the vector-boson-fusion channel the decays  $H \rightarrow WW \rightarrow l^\pm \nu jj$  can provide complimentary evidence in the intermediate Higgs-mass range  $140 \text{ GeV} < M_H < 200 \text{ GeV}$  [2, 8, 9] and constitute a good potential discovery channel in the medium-high Higgs-mass range  $M_H \gtrsim 300 \text{ GeV}$  [4]. At a linear collider, the hadronic and semileptonic final states are even more important since they allow for a full reconstruction of the Higgs-boson decay  $H \rightarrow WW$  [10].

A kinematical reconstruction of the Higgs-boson decays  $H \rightarrow WW \rightarrow 4f$  and the suppression of the corresponding backgrounds requires the study of distributions and the use of cuts defined from the kinematics of the decay fermions. In addition, the verification of the spin and of the CP properties of the Higgs boson relies on the study of angular, energy, and invariant-mass distributions [11]. These tasks require a Monte Carlo generator for  $H \rightarrow WW/ZZ \rightarrow 4f$ . Since the effects of radiative corrections, in particular real-photon or gluon radiation, are important, a Monte Carlo generator including all relevant corrections is needed.

The progress in the theoretical description of the decays of a SM Higgs boson into W- or Z-boson pairs has, for instance, been summarized in Ref. [12]. Until recently, calculations for off-shell vector bosons were only available in lowest order [13], and radiative corrections were known only in narrow-width approximation (NWA) [14], i.e. for on-shell W and Z bosons. In this case, also leading two-loop corrections enhanced by powers of the top-quark mass [15] or of the Higgs-boson mass [16] have been calculated. However, near and below the gauge-boson-pair thresholds the NWA is not applicable, so that only the lowest-order results existed in this  $M_H$  range.

In a recent paper [12] we have presented results for the complete electroweak (EW)  $\mathcal{O}(\alpha)$  corrections including some higher-order improvements to the Higgs-boson decays  $H \rightarrow WW/ZZ \rightarrow 4 \text{ leptons}$ . First results of this calculation had already been presented at the RADCOR05 conference [17]. At this conference also progress on an independent

calculation of the electromagnetic corrections to  $H \rightarrow ZZ \rightarrow 4$  leptons has been reported by Carloni Calame et al. [18]. The analytic results demonstrated in Ref. [12] are also valid for quarks in the final state. In this paper we supplement this calculation by the corresponding QCD corrections. We introduce a classification of the QCD corrections and describe their calculation. The QCD corrections have been implemented into the Monte Carlo generator PROPHECY4F, and numerical results have been produced. These include the partial widths for various semileptonic and hadronic channels as well as different invariant-mass and angular distributions for semileptonic final states.

The paper is organized as follows: In Section 2 we describe the setup of our calculation. Section 3 contains a classification of the QCD corrections and provides analytic results for the virtual and real QCD corrections. Numerical results are presented in Section 4, and our conclusions are given in Section 5.

## 2 Setup of the calculation

We consider the processes

$$H(p) \longrightarrow f_1(k_1, \sigma_1) + \bar{f}_2(k_2, \sigma_2) + f_3(k_3, \sigma_3) + \bar{f}_4(k_4, \sigma_4) + [\gamma/g(k, \lambda)], \quad (2.1)$$

where  $f_i$  stands for any lepton,  $l = e, \mu, \tau, \nu_e, \nu_\mu, \nu_\tau$ , or for any quark of the first two generations,  $q = d, u, s, c$ . We do not include final states with bottom or top quarks. The momenta and helicities of the external particles are indicated in parentheses. The helicities take the values  $\sigma_i = \pm 1/2$ , but we often use only the sign to indicate the helicity. The masses of the external fermions are neglected whenever possible, i.e. everywhere but in the mass-singular logarithms. We always sum over the four light quarks of the first two generations in the final state and set the CKM matrix to the unit matrix. This approximation ignores quark mixing with the third generation, which is, however, negligible.

The calculation of the EW corrections has already been described in Ref. [12], where results for purely leptonic final states have been discussed. Here we briefly repeat the salient features of the evaluation of virtual one-loop and real-photon corrections.

The calculation of the one-loop diagrams has been performed in the conventional 't Hooft–Feynman gauge and in the background-field formalism using the conventions of Refs. [19] and [20], respectively.

For the implementation of the finite widths of the gauge bosons we use the complex-mass scheme, which was introduced in Ref. [21] for lowest-order calculations and generalized to the one-loop level in Ref. [22]. In this approach the W- and Z-boson masses are consistently considered as complex quantities, defined as the locations of the propagator poles in the complex plane. The scheme fully respects all relations that follow from gauge invariance. A brief description of this scheme can also be found in Ref. [23].

The amplitudes have been generated with FEYNARTS, using the two independent versions 1 and 3, as described in Refs. [24] and [25], respectively. The algebraic evaluation has been performed in two completely independent ways. One calculation is based on an in-house program written in *Mathematica*, the other has been completed with the help of FORMCALC [26]. The amplitudes are expressed in terms of standard matrix elements and coefficients, which contain the tensor integrals, as described in the appendix of Ref. [27].

The tensor integrals are evaluated as in the calculation of the corrections to  $e^+e^- \rightarrow 4f$  [22, 28]. They are recursively reduced to master integrals at the numerical level. The scalar master integrals are evaluated for complex masses using the methods and results of Ref. [29]. UV divergences are regulated dimensionally and IR divergences with an infinitesimal photon mass. Tensor and scalar 5-point functions are directly expressed in terms of 4-point integrals [30]. Tensor 4-point and 3-point integrals are reduced to scalar integrals with the Passarino–Veltman algorithm [31] as long as no small Gram determinant appears in the reduction. If small Gram determinants occur, two alternative schemes are applied [32]. One method makes use of expansions of the tensor coefficients about the limit of vanishing Gram determinants and possibly other kinematical determinants. In the second, alternative method we evaluate a specific tensor coefficient, the integrand of which is logarithmic in Feynman parametrization, by numerical integration. Then the remaining coefficients as well as the standard scalar integral are algebraically derived from this coefficient. The results of the two different codes, based on the different methods described above are in good numerical agreement.

Since corrections due to the self-interaction of the Higgs boson become important for large Higgs-boson masses, we have included the dominant two-loop corrections to the decay  $H \rightarrow VV$  proportional to  $G_\mu^2 M_H^4$  in the large-Higgs-mass limit which were calculated in Ref. [16].

The matrix elements for the real-photon corrections are evaluated using the Weyl–van der Waerden spinor technique as formulated in Ref. [33] and have been checked against results obtained with MADGRAPH [34]. The soft and collinear singularities are treated both in the dipole subtraction method following Ref. [35] and in the phase-space slicing method following Ref. [36]. For the calculation of non-collinear-safe observables we use the extension of the subtraction method introduced in Ref. [37]. Final-state radiation beyond  $\mathcal{O}(\alpha)$  is included at the leading-logarithmic level using the structure functions given in Ref. [38] (see also references therein).

The phase-space integration is performed with Monte Carlo techniques. PROPHECY4F employs a multi-channel Monte Carlo generator [39] similar to the one implemented in RACOONWW [21] and COFFER $\gamma\gamma$  [37, 40]. Our second code uses the adaptive integration program VEGAS [41].

### 3 QCD corrections for $H \rightarrow 2q2l$ and $H \rightarrow 4q$

#### 3.1 Classification

A proper classification of QCD corrections is achieved upon considering possible contributions to the squared lowest-order amplitude. The amplitude itself receives contributions from one of the two tree diagrams shown in Figure 1 or from both. Thus, the square of this amplitude receives contributions from cut diagrams of the types depicted in Figure 2. Type (A) corresponds to the squares of each of the Born diagrams, type (B) to their interference if two Born diagrams exist.

After this preliminary consideration we define four different categories of QCD corrections. Examples of cut diagrams belonging to these categories are shown in Figure 3, the corresponding virtual QCD correction diagrams are depicted in Figure 4.

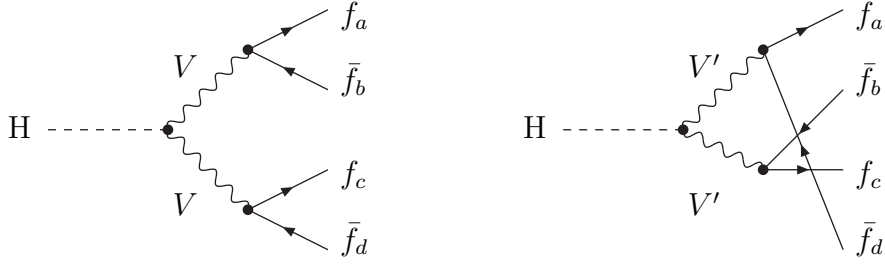


Figure 1: Possible lowest-order diagrams for  $H \rightarrow 4f$  where  $V, V' = W, Z$ .

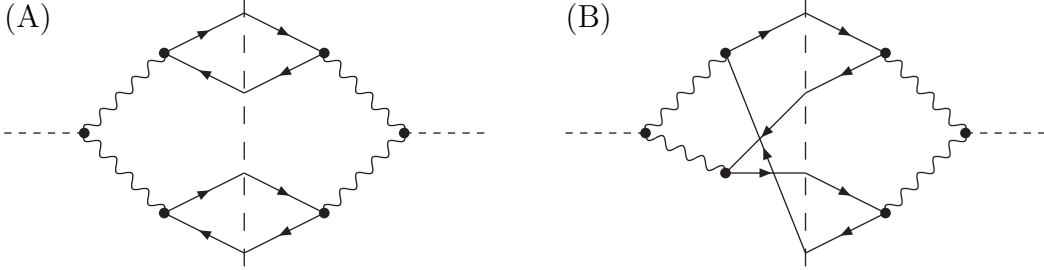


Figure 2: Types of cut diagrams contributing in lowest order.

- (a) *QCD corrections to gauge-boson decays* comprise all cut diagrams resulting from diagram (A) of Figure 2 by adding one additional gluon. Cut diagrams in which the gluon does not cross the cut correspond to virtual one-loop corrections, the one where the gluon crosses the cut correspond to real-gluon radiation. Note that cut diagrams in which the gluon connects the two closed quark lines identically vanish, because their colour structure is proportional to  $\text{Tr}(\lambda^h)\text{Tr}(\lambda^h) = 0$ , where  $\lambda^h$  is a Gell-Mann matrix. Thus, the only relevant one-loop diagrams in this category are gluonic vertex corrections to a weak-boson decay, as illustrated in the first diagram of Figure 4; the real corrections are induced by the corresponding gluon bremsstrahlung diagrams.

If a weak-boson decay is fully integrated over its decay angles, the resulting QCD correction of the considered type simply reduces to the well-known factor  $\alpha_s/\pi$  for a hadronically decaying vector boson.

- (b) *QCD corrections to interferences* comprise all cut diagrams resulting from diagram (B) of Figure 2 by adding one additional gluon, analogously to the previous category. Relevant one-loop diagrams are, thus, vertex corrections or pentagon diagrams, as illustrated in the first two diagrams of Figure 4.
- (c) *Corrections from intermediate  $q\bar{q}g^*$  states* are induced by loop diagrams exemplified by the third graph in Figure 4. The remaining graphs are obtained by shifting the gluon to different positions at the same quark line and by interchanging the role of the two quark lines. Thus, the diagrams comprise not only box diagrams but also vertex diagrams. They do not interfere with Born diagrams with the same fermion-

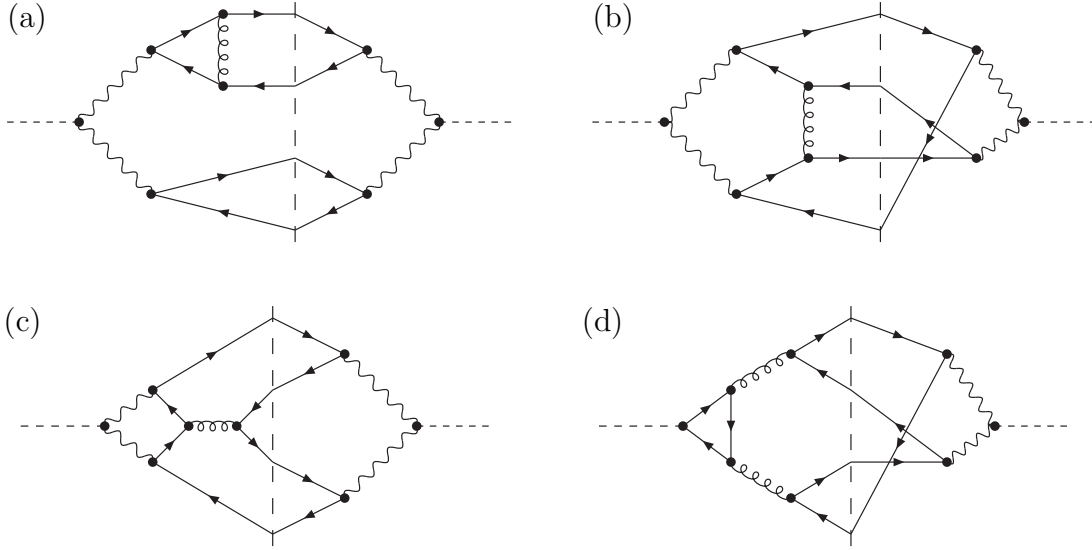


Figure 3: Categories of cut diagrams contributing to the QCD corrections.

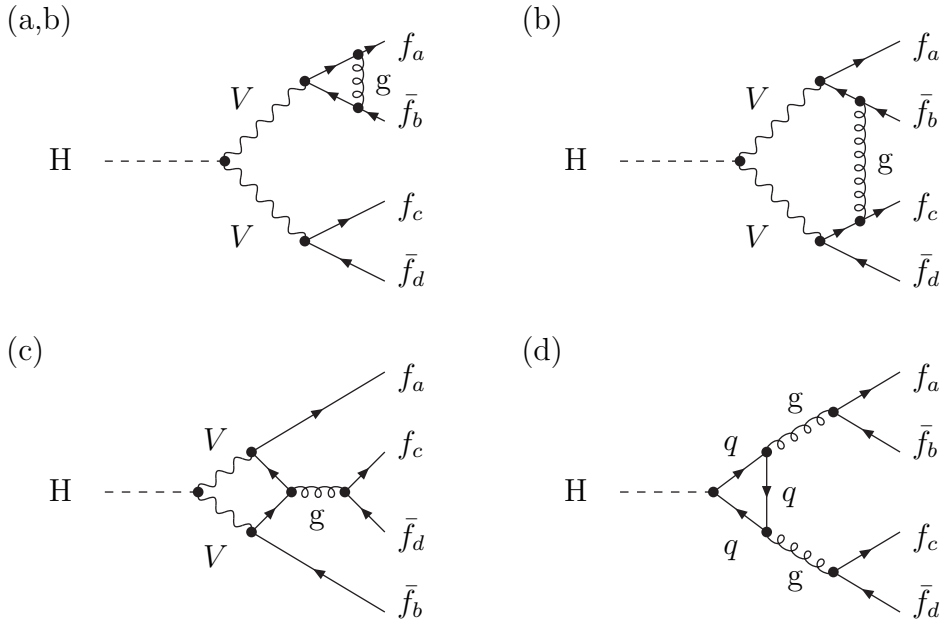


Figure 4: Basic diagrams contributing to the virtual QCD corrections for  $H \rightarrow 4f$  where  $V = W, Z$  and  $q = d, u, s, c, b, t$ . The categories of QCD corrections, (a)–(d), to which the diagrams contribute are indicated.

number flow because of the colour structure, i.e. in  $\mathcal{O}(\alpha_s)$  they only contribute if two Born diagrams exist.

Owing to the intermediate  $q\bar{q}g^*$  states, the squared diagrams of this category actually correspond to (collinear-singular) real NLO QCD corrections to the loop-induced decay  $H \rightarrow q\bar{q}g$ , where  $q$  is a massless quark. Here we consider only the interference contributions of the loop diagrams of this category with the lowest-order diagrams for the decay  $H \rightarrow VV \rightarrow 4q$ , resulting in a UV and IR (soft and collinear) finite correction.

- (d) *Corrections from intermediate  $g^*g^*$  states* are induced by diagrams exemplified by the fourth graph in Figure 4. There are precisely two graphs with opposite fermion-number flow in the loop. Again, owing to the colour structure (see also below), these diagrams do not interfere with Born diagrams with the same fermion-number flow, i.e. the existence of two Born diagrams is needed.

Owing to the intermediate  $g^*g^*$  states, the squared diagrams of this category actually correspond to (collinear-singular) real NNLO QCD corrections to the loop-induced decay  $H \rightarrow gg$ . The considered interference contributions of the loop diagrams of this category with the lowest-order diagrams for the decay  $H \rightarrow VV \rightarrow 4q$ , however, again yield a UV and IR (soft and collinear) finite correction.

From the classification, it is clear that category (a) exists for all final states involving quarks, while categories (b), (c), and (d) are only relevant for the hadronic decays  $H \rightarrow q\bar{q}q\bar{q}$  and  $H \rightarrow q\bar{q}q'\bar{q}'$ , where  $q$  and  $q'$  are weak-isospin partners. Categories (a), (b), and (c) give rise to contributions to the decay widths that are proportional to  $\alpha^3\alpha_s$ , while type (d) yields a contribution proportional to  $\alpha^2\alpha_s^2$ .

We do not consider the process  $H \rightarrow 4\text{jets}$  in general but only the contributions via virtual EW gauge-boson pairs, i.e. we assume that the gauge-boson resonances are isolated by experimental cuts. For the more inclusive decay  $H \rightarrow 4\text{jets}$ , also diagrams without intermediate EW gauge bosons, where the Higgs boson couples to gluons via heavy-quark loops, become important. Using an effective  $Hgg$  coupling, the calculation of the corresponding QCD one-loop matrix elements has been described in Ref. [42], but the full NLO QCD prediction for  $H \rightarrow 4\text{jets}$  including these effects is not yet available.

### 3.2 Virtual corrections

In the evaluation of the one-loop QCD diagrams, which are illustrated in Figure 4, the fermion spinor chains are separated from the rest of the amplitude by introducing 52 standard matrix elements  $\hat{\mathcal{M}}_i^{abcd,\sigma\tau}$ , as defined in Eq. (3.2) of Ref. [12], where the indices  $\sigma$  and  $\tau$  indicate the chiralities in the spinor chains of the fermion pairs  $f_a\bar{f}_b$  and  $f_c\bar{f}_d$ , respectively. Furthermore, the colour structure is extracted by defining the colour operators

$$C_1^{abcd} = \delta_{c_a c_b} \otimes \delta_{c_c c_d}, \quad C_2^{abcd} = \frac{1}{4C_F} \lambda_{c_a c_b}^h \otimes \lambda_{c_c c_d}^h = \frac{3}{16} \lambda_{c_a c_b}^h \otimes \lambda_{c_c c_d}^h \quad (3.1)$$

with the Gell-Mann matrices  $\lambda^h$ , the colour index  $h$  of the gluon, and the colour indices  $c_{a,b,c,d}$  of the quarks. For external leptons the corresponding colour index trivially takes

only one value, and the operator  $C_2$ , of course, appears only for four-quark final states. Using this notation, the generic lowest-order amplitude in colour space reads

$$\mathcal{A}_{0,c_a c_b c_c c_d}^{VV,\sigma_a \sigma_b \sigma_c \sigma_d}(k_a, k_b, k_c, k_d) = C_1^{abcd} \mathcal{M}_0^{VV,\sigma_a \sigma_b \sigma_c \sigma_d}(k_a, k_b, k_c, k_d), \quad (3.2)$$

where  $\mathcal{M}_0^{VV,\sigma_a \sigma_b \sigma_c \sigma_d}$  is the colour-stripped generic lowest-order amplitude defined in Eq. (2.7) of Ref. [12]. Obviously, this notation generalizes to the generic EW one-loop amplitudes (i.e. without gluon exchange) introduced in Eq. (3.3) of Ref. [12],<sup>1</sup>

$$\mathcal{A}_{\text{EW},c_a c_b c_c c_d}^{VV,\sigma_a \sigma_b \sigma_c \sigma_d} = C_1^{abcd} \mathcal{M}_{\text{EW}}^{VV,\sigma_a \sigma_b \sigma_c \sigma_d} = C_1^{abcd} \sum_{i=1}^{13} F_{\text{EW},i}^{abcd,\sigma_a \sigma_c} \hat{\mathcal{M}}_i^{abcd,\sigma_a \sigma_c} \delta_{\sigma_a, -\sigma_b} \delta_{\sigma_c, -\sigma_d}, \quad (3.3)$$

where  $\hat{\mathcal{M}}_i^{abcd,\sigma_a \sigma_c}$  denote the standard matrix elements and  $F_{\text{EW},i}^{abcd,\sigma_a \sigma_c}$  are Lorentz-invariant coefficient functions. In the generic amplitudes the superscript “VV” indicates the common fermion-number flow, which corresponds to the decays  $V \rightarrow f_a \bar{f}_b$  and  $V \rightarrow f_c \bar{f}_d$ . The one-loop QCD amplitude, which involves gluon exchange, receives contributions from both colour operators; in colour space we define

$$\begin{aligned} \mathcal{A}_{\text{QCD},c_a c_b c_c c_d}^{VV,\sigma_a \sigma_b \sigma_c \sigma_d} &= \sum_{j=1}^2 C_j^{abcd} \mathcal{M}_{\text{QCD},j}^{VV,\sigma_a \sigma_b \sigma_c \sigma_d}, \\ \mathcal{M}_{\text{QCD},j}^{VV,\sigma_a \sigma_b \sigma_c \sigma_d} &= \sum_{i=1}^{13} F_{\text{QCD},j,i}^{abcd,\sigma_a \sigma_c} \hat{\mathcal{M}}_i^{abcd,\sigma_a \sigma_c} \delta_{\sigma_a, -\sigma_b} \delta_{\sigma_c, -\sigma_d}, \end{aligned} \quad (3.4)$$

where the  $\mathcal{M}_{\text{QCD},j}^{VV,\sigma_a \sigma_b \sigma_c \sigma_d}$  are colour-stripped amplitudes.

From the generic matrix elements  $\mathcal{A}_{n,c_a c_b c_c c_d}^{VV,\sigma_a \sigma_b \sigma_c \sigma_d}$  ( $n = 0, 1$ ) the matrix elements  $\mathcal{A}_{n,c_a c_b c_c c_d}^{\sigma_a \sigma_b \sigma_c \sigma_d}$  for the specific processes are constructed as in Eqs. (2.11)–(2.14) of Ref. [12]. The index  $n = 1$  collectively represents the sum EW + QCD of EW and QCD one-loop contributions. We denote different fermions by  $f$  and  $F$ , and their weak-isospin partners by  $f'$  and  $F'$  ( $f \neq F, F'$ ). For purely hadronic final states the quarks are denoted by  $q$  and their weak-isospin partners by  $q'$ . Thus, we obtain:

- $\text{H} \rightarrow f \bar{f} F \bar{F}$ :

$$\mathcal{A}_{n,c_1 c_2 c_3 c_4}^{\sigma_1 \sigma_2 \sigma_3 \sigma_4}(k_1, k_2, k_3, k_4) = \mathcal{A}_{n,c_1 c_2 c_3 c_4}^{\text{ZZ},\sigma_1 \sigma_2 \sigma_3 \sigma_4}(k_1, k_2, k_3, k_4), \quad (3.5)$$

- $\text{H} \rightarrow f \bar{f}' F \bar{F}'$ :

$$\mathcal{A}_{n,c_1 c_2 c_3 c_4}^{\sigma_1 \sigma_2 \sigma_3 \sigma_4}(k_1, k_2, k_3, k_4) = \mathcal{A}_{n,c_1 c_2 c_3 c_4}^{\text{WW},\sigma_1 \sigma_2 \sigma_3 \sigma_4}(k_1, k_2, k_3, k_4), \quad (3.6)$$

- $\text{H} \rightarrow q \bar{q} q' \bar{q}'$ :

$$\begin{aligned} \mathcal{A}_{n,c_1 c_2 c_3 c_4}^{\sigma_1 \sigma_2 \sigma_3 \sigma_4}(k_1, k_2, k_3, k_4) &= \mathcal{A}_{n,c_1 c_2 c_3 c_4}^{\text{ZZ},\sigma_1 \sigma_2 \sigma_3 \sigma_4}(k_1, k_2, k_3, k_4) \\ &\quad - \mathcal{A}_{n,c_1 c_4 c_3 c_2}^{\text{ZZ},\sigma_1 \sigma_4 \sigma_3 \sigma_2}(k_1, k_4, k_3, k_2), \end{aligned} \quad (3.7)$$

---

<sup>1</sup>We note that the generic colour-stripped EW one-loop amplitude  $\mathcal{M}_{\text{EW}}^{VV,\sigma_a \sigma_b \sigma_c \sigma_d}$  was denoted  $\mathcal{M}_1^{abcd,\sigma\tau}$  in Eq. (3.3) of Ref. [12].



- $H \rightarrow q\bar{q}q'\bar{q}'$ :

$$\begin{aligned} \mathcal{A}_{n,c_1c_2c_3c_4}^{\sigma_1\sigma_2\sigma_3\sigma_4}(k_1, k_2, k_3, k_4) &= \mathcal{A}_{n,c_1c_2c_3c_4}^{ZZ,\sigma_1\sigma_2\sigma_3\sigma_4}(k_1, k_2, k_3, k_4) \\ &\quad - \mathcal{A}_{n,c_1c_4c_3c_2}^{WW,\sigma_1\sigma_4\sigma_3\sigma_2}(k_1, k_4, k_3, k_2). \end{aligned} \quad (3.8)$$

The relative signs between contributions of the basic subamplitudes to the full matrix elements account for the sign changes resulting from interchanging external fermion lines.

Since the lowest-order amplitudes only involve the colour operators  $C_1^{1234}$  and  $C_1^{1432}$ , the following colour sums appear in the calculation of squared lowest-order amplitudes and of interferences between one-loop and lowest-order matrix elements:

$$\begin{aligned} X_1^{(A)} &= \sum_{\{c_i\}} (C_1^{abcd} * C_1^{abcd}) = N_{f_a}^c N_{f_c}^c, & X_2^{(A)} &= \sum_{\{c_i\}} (C_1^{abcd} * C_2^{abcd}) = 0, \\ X_1^{(B)} &= \sum_{\{c_i\}} (C_1^{abcd} * C_1^{adcb}) = N_{f_a}^c, & X_2^{(B)} &= \sum_{\{c_i\}} (C_1^{abcd} * C_2^{adcb}) = N_{f_a}^c, \end{aligned} \quad (3.9)$$

where  $\sum_{\{c_i\}}$  stands for the sum over the colour indices  $c_a, c_b, c_c, c_d$ , and  $N_f^c$  is the colour factor for a fermion  $f$ , which is 1 for leptons and 3 for quarks.

Squared Born diagrams, as illustrated in type (A) of Figure 1, are proportional to  $X_1^{(A)}$ , lowest-order interference diagrams of type (B) are proportional to  $X_1^{(B)}$ . The situation is analogous for all one-loop diagrams without gluons. By definition, category (a) of the gluonic diagrams comprises all one-loop QCD corrections proportional to  $X_1^{(A)}$ . In category (b), the vertex corrections are proportional to  $X_1^{(B)}$  and the pentagons to  $X_2^{(B)}$ . Categories (c) and (d) receive only contributions from  $X_2^{(B)}$ ; interferences of one-loop diagrams like (c) and (d) in Figure 4 with Born diagrams of the same fermion-number flow vanish because of  $X_2^{(A)} = 0$ .

Finally, we obtain the following for the one-loop corrections to the squared matrix elements:

- $H \rightarrow f\bar{f}F\bar{F}$ :

$$\sum_{\{c_i\}} 2 \operatorname{Re} \left\{ \mathcal{A}_{0,c_1c_2c_3c_4}^{\sigma_1\sigma_2\sigma_3\sigma_4} * \mathcal{A}_{1,c_1c_2c_3c_4}^{\sigma_1\sigma_2\sigma_3\sigma_4} \right\} = 2 \operatorname{Re} \left\{ N_f^c N_F^c \mathcal{M}_0^{ZZ,\sigma_1\sigma_2\sigma_3\sigma_4} * \mathcal{M}_{\text{EW+QCD(a)}}^{ZZ,\sigma_1\sigma_2\sigma_3\sigma_4} \right\}, \quad (3.10)$$

- $H \rightarrow f\bar{f}'F\bar{F}'$ :

$$\sum_{\{c_i\}} 2 \operatorname{Re} \left\{ \mathcal{A}_{0,c_1c_2c_3c_4}^{\sigma_1\sigma_2\sigma_3\sigma_4} * \mathcal{A}_{1,c_1c_2c_3c_4}^{\sigma_1\sigma_2\sigma_3\sigma_4} \right\} = 2 \operatorname{Re} \left\{ N_f^c N_{F'}^c \mathcal{M}_0^{\text{WW},\sigma_1\sigma_2\sigma_3\sigma_4} * \mathcal{M}_{\text{EW+QCD(a)}}^{\text{WW},\sigma_1\sigma_2\sigma_3\sigma_4} \right\}, \quad (3.11)$$

- $H \rightarrow q\bar{q}q\bar{q}$ :

$$\begin{aligned} &\sum_{\{c_i\}} 2 \operatorname{Re} \left\{ \mathcal{A}_{0,c_1c_2c_3c_4}^{\sigma_1\sigma_2\sigma_3\sigma_4} * \mathcal{A}_{1,c_1c_2c_3c_4}^{\sigma_1\sigma_2\sigma_3\sigma_4} \right\} \\ &= 2 \operatorname{Re} \left\{ \mathcal{M}_0^{ZZ,\sigma_1\sigma_2\sigma_3\sigma_4} * \left[ (N_q^c)^2 \mathcal{M}_{\text{EW+QCD(a)}}^{ZZ,\sigma_1\sigma_2\sigma_3\sigma_4} - N_q^c \mathcal{M}_{\text{EW+QCD(b)+QCD(c)+QCD(d)}}^{ZZ,\sigma_1\sigma_4\sigma_3\sigma_2} \right] \right\} \\ &\quad + \left( q(k_2, \sigma_2) \leftrightarrow q(k_4, \sigma_4) \right), \end{aligned} \quad (3.12)$$

- $H \rightarrow q\bar{q}q'\bar{q}'$ :

$$\begin{aligned}
& \sum_{\{c_i\}} 2 \operatorname{Re} \left\{ \mathcal{A}_{0,c_1c_2c_3c_4}^{\sigma_1\sigma_2\sigma_3\sigma_4*} \mathcal{A}_{1,c_1c_2c_3c_4}^{\sigma_1\sigma_2\sigma_3\sigma_4} \right\} \\
&= 2 \operatorname{Re} \left\{ \mathcal{M}_0^{ZZ,\sigma_1\sigma_2\sigma_3\sigma_4*} \left[ (N_q^c)^2 \mathcal{M}_{EW+QCD(a)}^{ZZ,\sigma_1\sigma_2\sigma_3\sigma_4} - N_q^c \mathcal{M}_{EW+QCD(b)}^{WW,\sigma_1\sigma_4\sigma_3\sigma_2} \right] \right. \\
&\quad \left. + \mathcal{M}_0^{WW,\sigma_1\sigma_4\sigma_3\sigma_2*} \left[ (N_q^c)^2 \mathcal{M}_{EW+QCD(a)}^{WW,\sigma_1\sigma_4\sigma_3\sigma_2} \right. \right. \\
&\quad \left. \left. - N_q^c \mathcal{M}_{EW+QCD(b)+QCD(c)+QCD(d)}^{ZZ,\sigma_1\sigma_2\sigma_3\sigma_4} \right] \right\}. \quad (3.13)
\end{aligned}$$

Due to the electric charge flow, categories (c) and (d) only exist if there are corresponding diagrams with intermediate Z bosons. That is why there are no terms  $\mathcal{M}_0^{ZZ,\sigma_1\sigma_2\sigma_3\sigma_4*} \times \mathcal{M}_{QCD(c)+QCD(d)}^{WW,\sigma_1\sigma_4\sigma_3\sigma_2}$ . Note that in the notation we have suppressed the momentum arguments which, however, can be trivially restored, because the permutation of momenta  $k_i$  is the same as for the polarizations  $\sigma_i$  in each amplitude.

### 3.3 Matrix element for real-gluon emission $H \rightarrow 4fg$

The real-gluonic corrections are induced by the process

$$H(p) \longrightarrow f_1(k_1, \sigma_1) + \bar{f}_2(k_2, \sigma_2) + f_3(k_3, \sigma_3) + \bar{f}_4(k_4, \sigma_4) + g(k, \lambda), \quad (3.14)$$

where the momenta and helicities of the external particles are indicated in parentheses.

The matrix elements for this process can be constructed from the matrix elements for the photon radiation process  $\mathcal{M}_\gamma^{\sigma_a\sigma_b\sigma_c\sigma_d\lambda}(Q_a, Q_b, Q_c, Q_d, k_a, k_b, k_c, k_d, k)$ , which have been explicitly given in Ref. [12]. Here,  $Q_{a,b,c,d}$  denote the electric charges of the fermions. The generic amplitudes read

$$\begin{aligned}
& \mathcal{A}_{g,c_a c_b c_c c_d}^{VV,\sigma_a\sigma_b\sigma_c\sigma_d\lambda,h}(k_a, k_b, k_c, k_d, k) = \\
& \frac{g_s}{e} \left\{ \frac{1}{2} \lambda_{c_a c_b}^h \delta_{c_c c_d} \delta_{f_a q} \mathcal{M}_\gamma^{VV,\sigma_a\sigma_b\sigma_c\sigma_d\lambda}(1, 1, 0, 0, k_a, k_b, k_c, k_d, k) \right. \\
& \quad \left. + \frac{1}{2} \lambda_{c_c c_d}^h \delta_{c_a c_b} \delta_{f_c q} \mathcal{M}_\gamma^{VV,\sigma_a\sigma_b\sigma_c\sigma_d\lambda}(0, 0, 1, 1, k_a, k_b, k_c, k_d, k) \right\}, \quad (3.15)
\end{aligned}$$

where  $g_s$  is the strong coupling constant, and  $V = Z, W$  for Z-mediated and W-mediated decays, respectively. The symbols  $\delta_{f_i q}$  are equal to one if  $f_i$  is a quark and zero otherwise.

From the generic matrix element  $\mathcal{A}_{g,c_a c_b c_c c_d}^{VV,\sigma_a\sigma_b\sigma_c\sigma_d\lambda,h}(k_a, k_b, k_c, k_d, k)$  the matrix elements for the specific processes can be constructed as follows. As above, we denote different fermions ( $f \neq F, F'$ ) by  $f$  and  $F$ , and their weak-isospin partners by  $f'$  and  $F'$ , respectively:

- $H \rightarrow f\bar{f}F\bar{F}g$ :

$$\mathcal{A}_{g,c_1c_2c_3c_4}^{\sigma_1\sigma_2\sigma_3\sigma_4\lambda,h}(k_1, k_2, k_3, k_4, k) = \mathcal{A}_{g,c_1c_2c_3c_4}^{ZZ,\sigma_1\sigma_2\sigma_3\sigma_4\lambda,h}(k_1, k_2, k_3, k_4, k), \quad (3.16)$$

- $H \rightarrow f\bar{f}'F\bar{F}'g$ :

$$\mathcal{A}_{g,c_1c_2c_3c_4}^{\sigma_1\sigma_2\sigma_3\sigma_4\lambda,h}(k_1, k_2, k_3, k_4, k) = \mathcal{A}_{g,c_1c_2c_3c_4}^{WW,\sigma_1\sigma_2\sigma_3\sigma_4\lambda,h}(k_1, k_2, k_3, k_4, k), \quad (3.17)$$

- $H \rightarrow q\bar{q}q\bar{q}g$ :

$$\begin{aligned} \mathcal{A}_{g,c_1c_2c_3c_4}^{\sigma_1\sigma_2\sigma_3\sigma_4\lambda,h}(k_1, k_2, k_3, k_4, k) &= \mathcal{A}_{g,c_1c_2c_3c_4}^{ZZ,\sigma_1\sigma_2\sigma_3\sigma_4\lambda,h}(k_1, k_2, k_3, k_4, k) \\ &\quad - \mathcal{A}_{g,c_1c_4c_3c_2}^{ZZ,\sigma_1\sigma_4\sigma_3\sigma_2\lambda,h}(k_1, k_4, k_3, k_2, k), \end{aligned} \quad (3.18)$$

- $H \rightarrow q\bar{q}q'\bar{q}'g$ :

$$\begin{aligned} \mathcal{A}_{g,c_1c_2c_3c_4}^{\sigma_1\sigma_2\sigma_3\sigma_4\lambda,h}(k_1, k_2, k_3, k_4, k) &= \mathcal{A}_{g,c_1c_2c_3c_4}^{ZZ,\sigma_1\sigma_2\sigma_3\sigma_4\lambda,h}(k_1, k_2, k_3, k_4, k) \\ &\quad - \mathcal{A}_{g,c_1c_4c_3c_2}^{WW,\sigma_1\sigma_4\sigma_3\sigma_2\lambda,h}(k_1, k_4, k_3, k_2, k). \end{aligned} \quad (3.19)$$

The relative signs between contributions of the basic subamplitudes to the full matrix elements account for the sign changes resulting from interchanging external fermion lines.

Squaring the amplitudes and summing over the colour degrees of freedom, we have

- $H \rightarrow f\bar{f}F\bar{F}g$ :

$$\begin{aligned} \sum_{\{c_i\},h} \left| \mathcal{A}_{g,c_1c_2c_3c_4}^{\sigma_1\sigma_2\sigma_3\sigma_4\lambda,h}(k_1, k_2, k_3, k_4, k) \right|^2 &= \frac{4}{3} N_f^c N_F^c \frac{\alpha_s}{\alpha} \\ &\quad \times \left[ \delta_{fq} \left| \mathcal{M}_\gamma^{ZZ,\sigma_1\sigma_2\sigma_3\sigma_4\lambda}(1, 1, 0, 0, k_1, k_2, k_3, k_4, k) \right|^2 \right. \\ &\quad \left. + \delta_{Fq} \left| \mathcal{M}_\gamma^{ZZ,\sigma_1\sigma_2\sigma_3\sigma_4\lambda}(0, 0, 1, 1, k_1, k_2, k_3, k_4, k) \right|^2 \right], \end{aligned} \quad (3.20)$$

- $H \rightarrow f\bar{f}'F\bar{F}'g$ :

$$\begin{aligned} \sum_{\{c_i\},h} \left| \mathcal{A}_{g,c_1c_2c_3c_4}^{\sigma_1\sigma_2\sigma_3\sigma_4\lambda,h}(k_1, k_2, k_3, k_4, k) \right|^2 &= \frac{4}{3} N_f^c N_F^c \frac{\alpha_s}{\alpha} \\ &\quad \times \left[ \delta_{fq} \left| \mathcal{M}_\gamma^{WW,\sigma_1\sigma_2\sigma_3\sigma_4\lambda}(1, 1, 0, 0, k_1, k_2, k_3, k_4, k) \right|^2 \right. \\ &\quad \left. + \delta_{Fq} \left| \mathcal{M}_\gamma^{WW,\sigma_1\sigma_2\sigma_3\sigma_4\lambda}(0, 0, 1, 1, k_1, k_2, k_3, k_4, k) \right|^2 \right], \end{aligned} \quad (3.21)$$

- $H \rightarrow q\bar{q}q\bar{q}g$ :

$$\begin{aligned} \sum_{\{c_i\},h} \left| \mathcal{A}_{g,c_1c_2c_3c_4}^{\sigma_1\sigma_2\sigma_3\sigma_4\lambda,h}(k_1, k_2, k_3, k_4, k) \right|^2 &= \frac{4}{3} (N_q^c)^2 \frac{\alpha_s}{\alpha} \\ &\quad \times \left[ \left| \mathcal{M}_\gamma^{ZZ,\sigma_1\sigma_2\sigma_3\sigma_4\lambda}(1, 1, 0, 0, k_1, k_2, k_3, k_4, k) \right|^2 \right. \\ &\quad + \left| \mathcal{M}_\gamma^{ZZ,\sigma_1\sigma_2\sigma_3\sigma_4\lambda}(0, 0, 1, 1, k_1, k_2, k_3, k_4, k) \right|^2 \\ &\quad + \left| \mathcal{M}_\gamma^{ZZ,\sigma_1\sigma_4\sigma_3\sigma_2\lambda}(1, 1, 0, 0, k_1, k_4, k_3, k_2, k) \right|^2 \\ &\quad \left. + \left| \mathcal{M}_\gamma^{ZZ,\sigma_1\sigma_4\sigma_3\sigma_2\lambda}(0, 0, 1, 1, k_1, k_4, k_3, k_2, k) \right|^2 \right] \\ &\quad - \frac{8}{3} N_q^c \frac{\alpha_s}{\alpha} \operatorname{Re} \left[ \left( \mathcal{M}_\gamma^{ZZ,\sigma_1\sigma_2\sigma_3\sigma_4\lambda}(1, 1, 0, 0, k_1, k_2, k_3, k_4, k) \right) \right. \end{aligned}$$

$$\begin{aligned}
& + \mathcal{M}_\gamma^{ZZ,\sigma_1\sigma_2\sigma_3\sigma_4\lambda}(0, 0, 1, 1, k_1, k_2, k_3, k_4, k) \Big)^* \\
& \times \left( \mathcal{M}_\gamma^{ZZ,\sigma_1\sigma_4\sigma_3\sigma_2\lambda}(1, 1, 0, 0, k_1, k_4, k_3, k_2, k) \right. \\
& \left. + \mathcal{M}_\gamma^{ZZ,\sigma_1\sigma_4\sigma_3\sigma_2\lambda}(0, 0, 1, 1, k_1, k_4, k_3, k_2, k) \right) \Big], \tag{3.22}
\end{aligned}$$

•  $H \rightarrow q\bar{q}q'q'g$ :

$$\begin{aligned}
& \sum_{\{c_i\},h} \left| \mathcal{A}_{g,c_1c_2c_3c_4}^{\sigma_1\sigma_2\sigma_3\sigma_4\lambda,h}(k_1, k_2, k_3, k_4, k) \right|^2 = \frac{4}{3} (N_q^c)^2 \frac{\alpha_s}{\alpha} \\
& \times \left[ \left| \mathcal{M}_\gamma^{ZZ,\sigma_1\sigma_2\sigma_3\sigma_4\lambda}(1, 1, 0, 0, k_1, k_2, k_3, k_4, k) \right|^2 \right. \\
& + \left| \mathcal{M}_\gamma^{ZZ,\sigma_1\sigma_2\sigma_3\sigma_4\lambda}(0, 0, 1, 1, k_1, k_2, k_3, k_4, k) \right|^2 \\
& + \left| \mathcal{M}_\gamma^{WW,\sigma_1\sigma_4\sigma_3\sigma_2\lambda}(1, 1, 0, 0, k_1, k_4, k_3, k_2, k) \right|^2 \\
& + \left. \left| \mathcal{M}_\gamma^{WW,\sigma_1\sigma_4\sigma_3\sigma_2\lambda}(0, 0, 1, 1, k_1, k_4, k_3, k_2, k) \right|^2 \right] \\
& - \frac{8}{3} N_q^c \frac{\alpha_s}{\alpha} \operatorname{Re} \left[ \left( \mathcal{M}_\gamma^{ZZ,\sigma_1\sigma_2\sigma_3\sigma_4\lambda}(1, 1, 0, 0, k_1, k_2, k_3, k_4, k) \right. \right. \\
& \left. \left. + \mathcal{M}_\gamma^{ZZ,\sigma_1\sigma_2\sigma_3\sigma_4\lambda}(0, 0, 1, 1, k_1, k_2, k_3, k_4, k) \right)^* \right. \\
& \times \left( \mathcal{M}_\gamma^{WW,\sigma_1\sigma_4\sigma_3\sigma_2\lambda}(1, 1, 0, 0, k_1, k_4, k_3, k_2, k) \right. \\
& \left. \left. + \mathcal{M}_\gamma^{WW,\sigma_1\sigma_4\sigma_3\sigma_2\lambda}(0, 0, 1, 1, k_1, k_4, k_3, k_2, k) \right) \right]. \tag{3.23}
\end{aligned}$$

The contribution  $\Gamma_g$  of the radiative decay to the total decay width is given by

$$\Gamma_g = \frac{1}{2M_H} \int d\Phi_g \sum_{\{c_i\},h} \sum_{\{\sigma_i\},\lambda=\pm 1} \left| \mathcal{A}_{g,c_1c_2c_3c_4}^{\sigma_1\sigma_2\sigma_3\sigma_4\lambda,h} \right|^2, \tag{3.24}$$

where the phase-space integral is defined by

$$\int d\Phi_g = \int \frac{d^3\mathbf{k}}{(2\pi)^3 2k^0} \left( \prod_{i=1}^4 \int \frac{d^3\mathbf{k}_i}{(2\pi)^3 2k_i^0} \right) (2\pi)^4 \delta \left( p - k - \sum_{j=1}^4 k_j \right). \tag{3.25}$$

## 4 Numerical results

### 4.1 Setup and input

We use the  $G_\mu$  scheme, i.e. we define the electromagnetic coupling by  $\alpha_{G_\mu} = \sqrt{2}G_\mu M_W^2(1 - M_W^2/M_Z^2)/\pi$ . Our lowest-order results include the  $\mathcal{O}(\alpha)$ -corrected width of the gauge bosons. In the QCD corrections we uniformly take a fixed value for  $\alpha_s = \alpha_s(M_Z) = 0.1187$  everywhere, because the only numerically relevant part (see below) of the QCD correction is the one connected with the hadronic decay of a W or a Z boson, where the scale is fixed by the intermediate gauge-boson decay. More details about the setup and all input parameters are provided in Ref. [12].

In our approach the final states involve either four fermions (from lowest order and virtual corrections), four fermions and a photon (from real-photon corrections), four fermions and a gluon (from real-gluon corrections), or four fermions and one or more photons collinear to an outgoing lepton (from the structure functions describing multi-photon final-state radiation). In particular there are no events containing both photons and gluons. Moreover, we only consider semileptonic final states in the distributions. For these distributions, a photon and gluon recombination is performed as follows. In events with a real photon, as in Ref. [12] the photon is recombined with the (in this sense) nearest charged fermion if the invariant mass of the photon-fermion pair is below 5 GeV. This, in particular, implies that all photons collinear to a lepton are recombined with the corresponding lepton if the recombination is switched on (as always done in the results of this paper), i.e. the higher-order effects from photonic final-state radiation described in Section 4.3 of Ref. [12] fully cancel out in this case. In the case of real-gluon radiation we force a 2-jet event. This is achieved by always recombining the two partons of the  $q\bar{q}g$  system that yield the smallest invariant mass. Invariant masses and angles are then defined by the 4-momenta of the recombined pair and the remaining partons.

We always sum over the quarks of the first two generations,  $q = u, d, c, s$ , and over the three neutrinos in the final states and we consider the final states  $eeqq$ ,  $\nu\nu qq$ ,  $e\nu qq$ , and  $qqqq$ . Since we consistently neglect the masses of external fermions and average over polarizations, we can express the partial widths of these final states as

$$\begin{aligned}
\Gamma_{H\rightarrow eeqq} &= 2\Gamma_{H\rightarrow e^-e^+u\bar{u}} + 2\Gamma_{H\rightarrow e^-e^+d\bar{d}}, \\
\Gamma_{H\rightarrow \nu\nu qq} &= 6\Gamma_{H\rightarrow \nu_e\bar{\nu}_e u\bar{u}} + 6\Gamma_{H\rightarrow \nu_e\bar{\nu}_e d\bar{d}}, \\
\Gamma_{H\rightarrow e\nu qq} &= 4\Gamma_{H\rightarrow e^-\bar{\nu}_e u\bar{d}}, \\
\Gamma_{H\rightarrow qqqq} &= \Gamma_{H\rightarrow u\bar{u}c\bar{c}} + \Gamma_{H\rightarrow d\bar{d}s\bar{s}} + 2\Gamma_{H\rightarrow u\bar{u}s\bar{s}} + 2\Gamma_{H\rightarrow u\bar{d}s\bar{c}} \\
&\quad + 2\Gamma_{H\rightarrow u\bar{d}d\bar{u}} + 2\Gamma_{H\rightarrow u\bar{u}u\bar{u}} + 2\Gamma_{H\rightarrow d\bar{d}d\bar{d}}.
\end{aligned} \tag{4.1}$$

Note that  $\Gamma_{H\rightarrow e\nu qq}$  includes both electrons and positrons in the final state. The partial widths with muons in the final state can be classified in the same way and are equal to those with the muons replaced by electrons, because no dependence on the final-state fermion masses remains for these inclusive quantities.

The results for the partial decay widths in the plots are calculated using  $10^7$  Monte Carlo events, while all other results (decay widths in the table and distribution plots) are obtained with  $5 \times 10^7$  events. In the presented results, soft and collinear divergences are treated with the dipole-subtraction method and have been checked by applying the phase-space slicing method. For the latter method more Monte Carlo events are needed for an accuracy at the per-mille level, because the energy and angular cuts in this method have to be chosen small enough rendering the real corrections and the analytically integrated soft and collinear singular contribution (which compensate each other) very large. In both methods it is possible to evaluate the virtual corrections (rendered finite by adding the soft and collinear singularities from the real corrections) less often than the lowest-order matrix elements, because the virtual corrections and also their statistical error are smaller. We evaluate the EW virtual corrections only every 100th time and the virtual QCD corrections only every 20th time. This procedure reduces the run-time of the program while maintaining the size of the overall statistical error.

	$M_H$ [GeV]	140		170		200	
	$\Gamma_W$ [GeV]	2.09052...		2.09054...		2.09055...	
	$\Gamma_Z$ [GeV]	2.50278...		2.50287...		2.50292...	
H $\rightarrow$		$\Gamma$ [MeV]	$\delta$ [%]	$\Gamma$ [MeV]	$\delta$ [%]	$\Gamma$ [MeV]	$\delta$ [%]
$eeqq$	corrected	0.020467(6)	5.1	0.32723(9)	5.7	13.332(2)	7.6
	EW	0.019731(5)	1.3	0.31558(7)	2.0	12.863(1)	3.8
	QCD	0.020217(5)	3.8	0.32115(7)	3.8	12.858(1)	3.8
	LO	0.019481(4)		0.30950(5)		12.389(1)	
$\nu\nu qq$	corrected	0.12221(4)	5.9	1.9559(6)	6.7	79.69(1)	8.5
	EW	0.11784(3)	2.1	1.8873(4)	2.9	76.91(1)	4.8
	QCD	0.11982(3)	3.8	1.9025(5)	3.7	76.20(1)	3.8
	LO	0.11545(3)		1.8339(4)		73.423(8)	
$e\nu qq$	corrected	0.5977(3)	7.4	53.55(2)	9.9	155.37(4)	8.7
	EW	0.5767(2)	3.6	51.71(1)	6.1	149.96(3)	4.9
	QCD	0.5775(2)	3.8	50.57(1)	3.8	148.32(3)	3.8
	LO	0.5564(2)		48.724(9)		142.91(2)	
$qqqq$	corrected	2.0113(8)	10.8	168.73(5)	13.6	590.3(1)	12.1
	EW	1.8752(4)	3.3	157.50(2)	6.0	550.47(7)	4.6
	QCD	1.9511(7)	7.5	159.83(4)	7.6	566.2(1)	7.6
	LO	1.8150(4)		148.59(2)		526.39(5)	

Table 1: Partial decay widths  $\Gamma_{H\rightarrow 4f}$  in lowest order (LO), including  $\mathcal{O}(\alpha)$  and  $\mathcal{O}(G_\mu^2 M_H^4)$  EW corrections,  $\mathcal{O}(\alpha_s)$  QCD corrections, and the sum of EW and QCD corrections (corrected) and corresponding relative corrections  $\delta$  for semileptonic and hadronic decay channels and different Higgs-boson masses.

## 4.2 Results for partial decay widths

In Table 1 we show the partial decay widths of the Higgs boson for semileptonic and hadronic final states for different values of the Higgs-boson mass. We list the lowest-order (LO) predictions and the predictions including the complete EW  $\mathcal{O}(\alpha)$  plus  $\mathcal{O}(G_\mu^2 M_H^4)$  corrections and the  $\mathcal{O}(\alpha_s)$  QCD corrections. In addition we give the predictions including only the EW corrections and only the QCD corrections. In all cases we provide also the relative corrections  $\delta = \Gamma/\Gamma_0 - 1$  in per cent. The statistical errors of the phase-space integration are given in parentheses. The size of the EW corrections is very similar to the size of the corresponding corrections for leptonic final states discussed in Ref. [12]. Since the QCD corrections mainly arise from vertex corrections and since we consider the integrated partial widths, the QCD contribution roughly amounts to  $\alpha_s/\pi$  for semileptonic final states and  $2\alpha_s/\pi$  for the hadronic final state. The sum of EW and QCD corrections thus rises to 5–14%.

In Figures 5, 6, and 7 we show the partial decay widths as a function of the Higgs-boson mass for  $H \rightarrow eeqq$ ,  $H \rightarrow e\nu qq$ , and  $H \rightarrow qqqq$ , respectively. The upper plots show the predictions including both QCD and EW corrections. The lower plots depict the corrections relative to the lowest order. Besides the EW+QCD corrections, these plots include the EW and QCD corrections separately, the narrow-width approximation (NWA) and the improved Born approximation (IBA) as defined in Eqs. (7.5)–(7.7) and Eqs. (6.1)–(6.7), respectively, of Ref. [12]. We recall that the IBA for the partial decay widths includes leading effects such as corrections that are enhanced by factors  $G_\mu m_t^2$  or  $G_\mu M_H^2$ , the Coulomb singularity for W pairs near their on-shell threshold, and the QCD correction to hadronically decaying gauge bosons. Apart from these effects, the IBA contains only one fitted constant for the WW- and ZZ-mediated channels each. Both in the WW-induced channel and in the ZZ-induced channel the EW corrections are very similar to the corresponding corrections for leptonic final states [12]. For moderate Higgs-boson mass, they are positive and below  $\sim 4\%$  for decays via Z pairs. For the W-mediated decays the Coulomb singularity yields a large effect near the WW threshold and the EW corrections are in the range between 2% and 8% for moderate Higgs-boson mass. For all decays the EW corrections reach about 13% near  $M_H = 700$  GeV. The thresholds for the on-shell decay of the Higgs boson into W bosons, Z bosons, and top quarks are manifest in the shape of the corrections. The QCD corrections amount to roughly  $\alpha_s/\pi \approx 3.8\%$  for semileptonic and  $2\alpha_s/\pi \approx 7.6\%$  for hadronic final states and are practically independent of the Higgs-boson mass. For  $H \rightarrow eeqq$  the agreement between the full result and the NWA is (accidentally) at the per-mille level sufficiently above the ZZ threshold. For  $H \rightarrow e\nu qq$  and  $H \rightarrow qqqq$  the NWA agrees with the full results within 1–2% above threshold. The IBA describes the full corrections within 2–3% for  $M_H \lesssim 400$  GeV for all final states.

In Section 3.1 we defined a classification of QCD corrections for the four-quark final states. While only category (a), i.e. QCD corrections to gauge-boson decays, exists for the final states  $H \rightarrow q\bar{q}Q\bar{Q}$  and  $H \rightarrow q\bar{q}'Q\bar{Q}'$  ( $q \neq Q, Q'$ ), all categories (a)–(d) contribute to  $H \rightarrow q\bar{q}q\bar{q}$  and  $H \rightarrow q\bar{q}q'\bar{q}'$ . Figure 8 shows the relative EW corrections and the subcontributions of the different categories of QCD corrections as a function of the Higgs-boson mass. The corrections to gauge-boson decays, i.e. category (a), make up practically all of the QCD part. Note that the contributions (b)–(d) are multiplied by a factor 10 in the plots. For  $M_H \gtrsim 2M_W$ , these contributions are completely negligible. In this region they are suppressed by a factor  $(\Gamma_V/M_V)^2$  with respect to the leading contributions because they have two propagators less that can become resonant. Below the WW threshold this suppression becomes smaller but at  $M_H = 120$  GeV the interference contribution is still rather small reaching only a few per mille. The largest corrections originate from intermediate  $g^*g^*$  states [category (d)], because these corrections are proportional to  $\alpha^2\alpha_s^2$  rather than to  $\alpha^3\alpha_s$  as all other QCD corrections.

### 4.3 Invariant-mass distributions

In order to reconstruct the Higgs-decay events and in order to separate signal events from possible background events, distributions in the invariant mass of fermion pairs resulting from a W- or Z-boson decay should be investigated. On the l.h.s. of Figure 9 we show the invariant-mass distribution of the  $qq$  pair in the decay  $H \rightarrow eeqq$  including QCD and EW corrections for  $M_H = 170$  GeV and  $M_H = 200$  GeV, i.e. for one  $M_H$  value

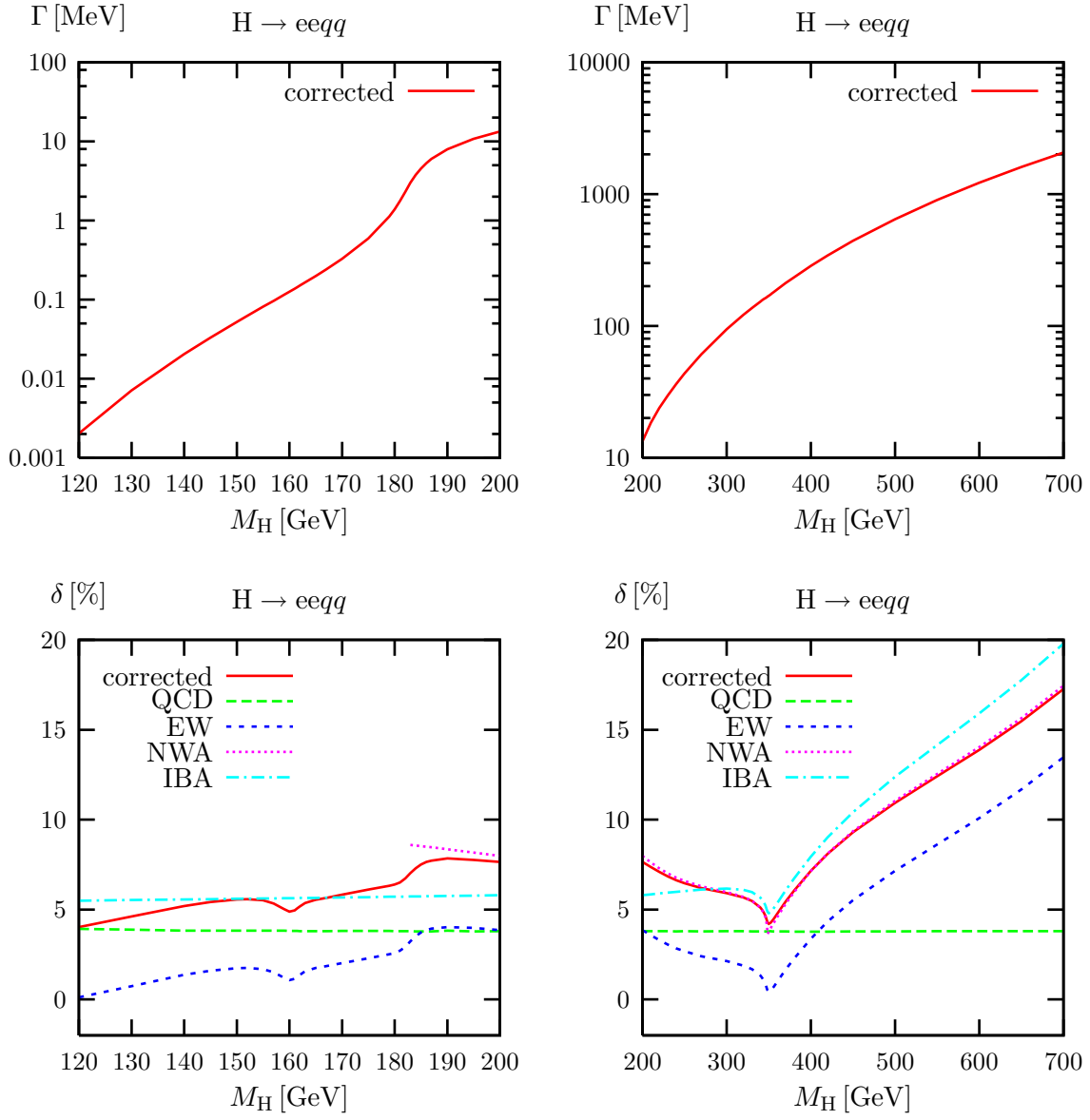


Figure 5: Partial decay width for  $H \rightarrow eeqq$  as a function of the Higgs-boson mass. The upper plots show the absolute prediction including QCD and EW corrections, and the lower plots show the relative size of the QCD and EW corrections separately, their sum (corrected) and the predictions of the NWA and the IBA.



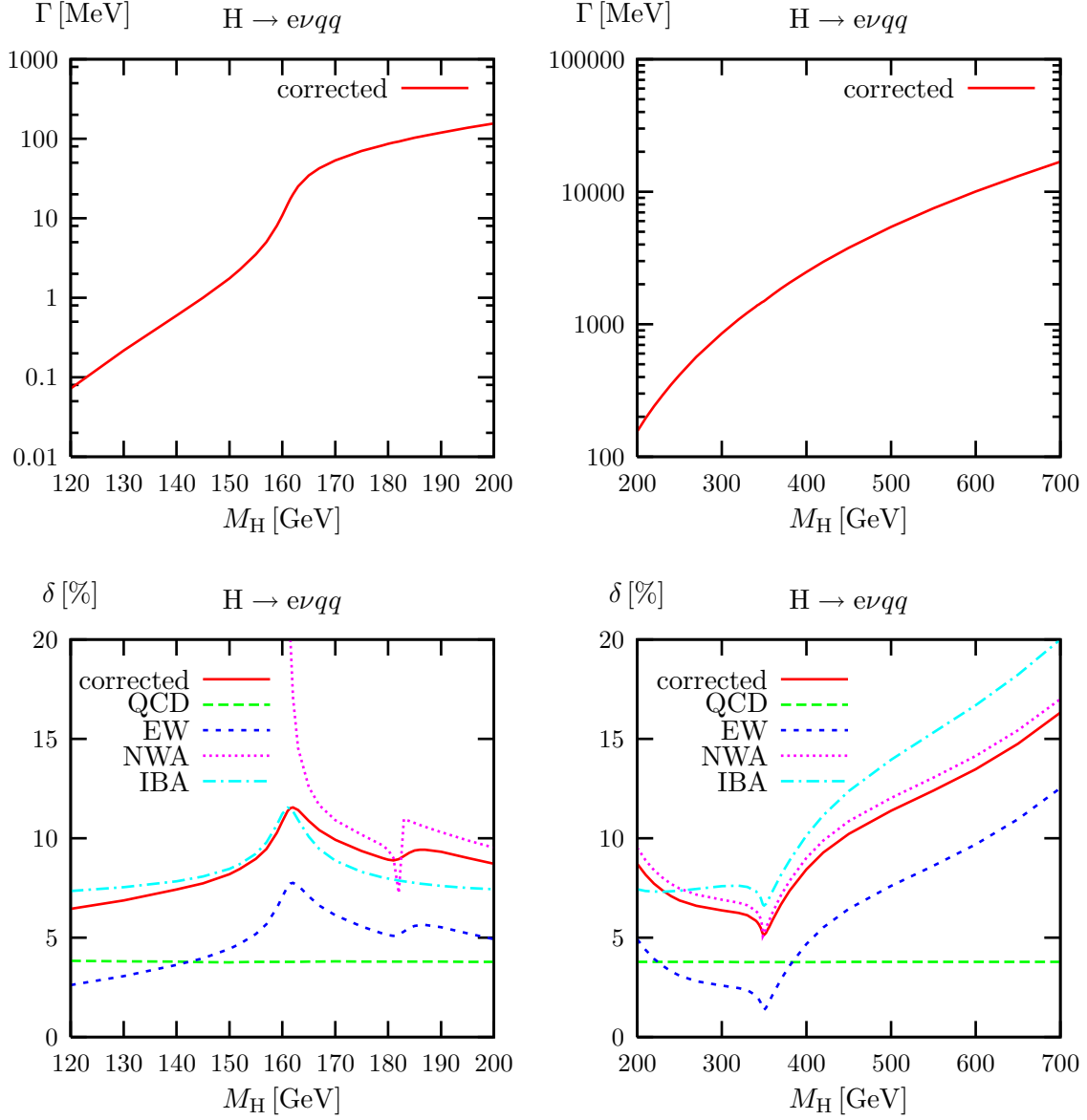


Figure 6: Partial decay width for  $H \rightarrow e\nu qq$  as a function of the Higgs-boson mass. The individual curves are defined as in Figure 5.

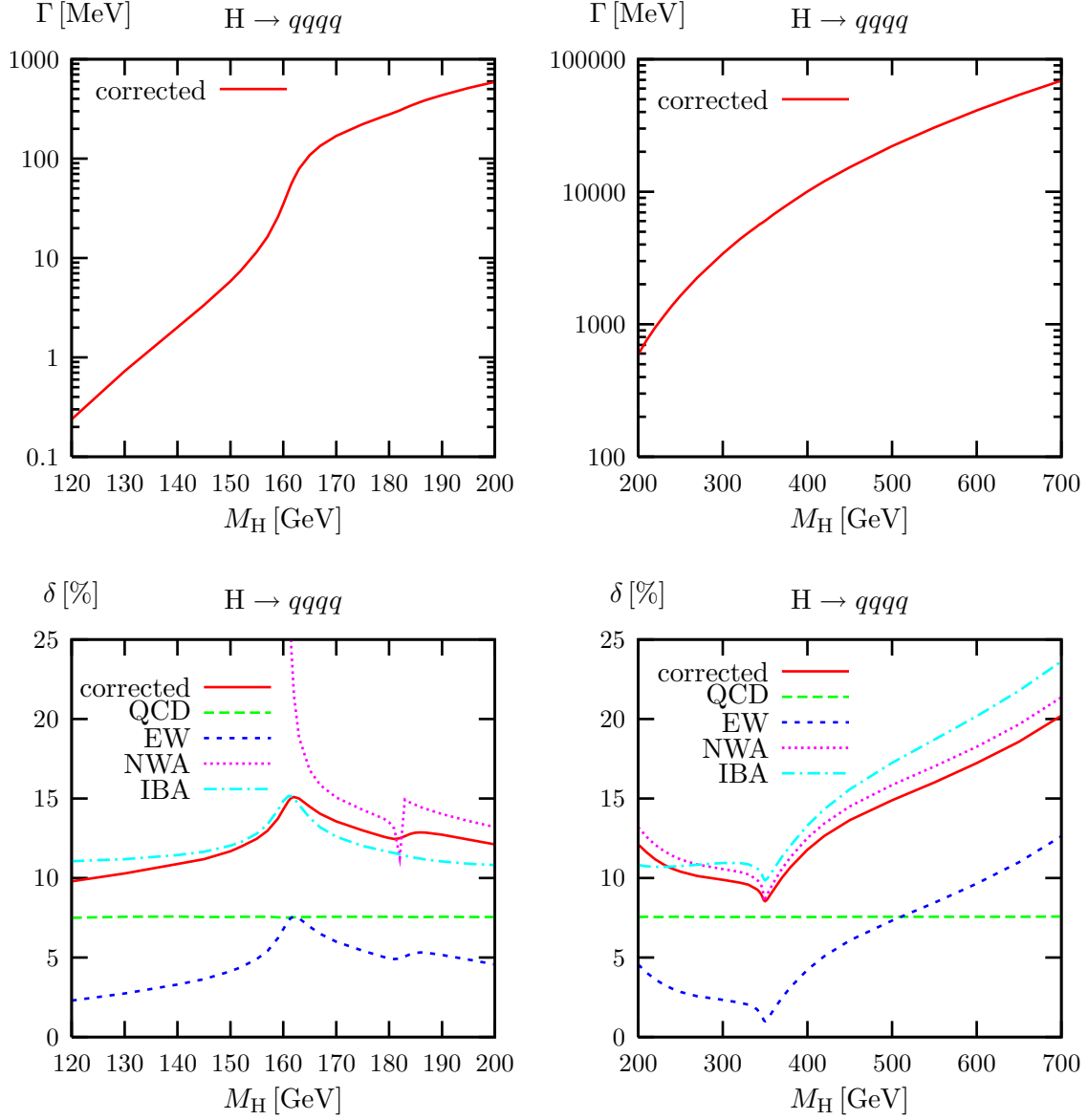


Figure 7: Partial decay width for  $H \rightarrow qqqq$  as a function of the Higgs-boson mass. The individual curves are defined as in Figure 5.

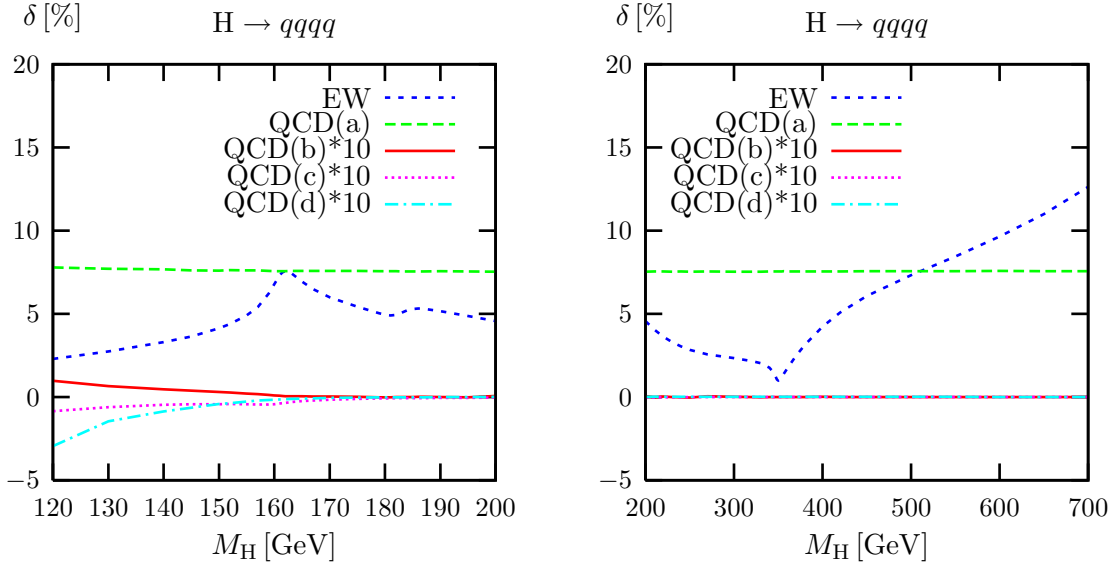


Figure 8: Comparison of the different QCD contributions defined in Section 3.1 and the EW contribution to the corrections to the partial decay width for  $H \rightarrow qq\bar{q}\bar{q}$  as a function of the Higgs-boson mass.

below and another above the on-shell threshold at  $2M_Z$  for Z-boson pairs. Above the threshold for the on-shell decay into a Z-boson pair there is just a resonance around the Z-boson mass. Below the threshold only one Z boson can become resonant while the other Z boson is off shell. Hence, in addition to the peak around the Z-boson mass, the  $qq$  invariant-mass distribution shows an enhancement for  $M_{qq} < M_H - M_Z \approx 80$  GeV where the  $e^+e^-$  pair can result from a resonant Z boson.

The complete relative corrections to the distribution in the invariant mass of the  $qq$  pair and also of the  $e^+e^-$  pair are shown on the r.h.s. of Figure 9. In addition, the QCD corrections to the  $M_{qq}$  distribution are plotted separately; they are flat and amount to roughly 3.8%. Note that  $M_{qq}$  actually is the total hadronic invariant mass resulting from the  $H \rightarrow eeqq$  decay, since we always recombine the  $q\bar{q}(g)$  system to two jets. In a detailed experimental analysis a jet algorithm should be defined. Then, hard gluons can produce a separate jet and the QCD corrections need not be flat anymore. For such a study, the jet algorithm could simply be interfaced to our Monte Carlo program. The EW corrections reveal the same structure as discussed in the case of leptonic decays [12] shifting the peak position of the resonance. Close to the resonance and above, the EW corrections can reach 5–10%, below the resonance they become larger. The dominant effect is of photonic origin, leading to more pronounced corrections in the case of the leptonic invariant mass  $M_{e^+e^-}$ , since the electric-charge factors are larger for leptons than for quarks. The way photons are treated has a strong impact on the corrections. By performing photon recombination, as defined in Section 4.1, we obtain collinear-safe observables. Thus, the corrections are of moderate size. However, for non-collinear-safe observables, i.e. if no photon recombination with leptons were performed, the corrections

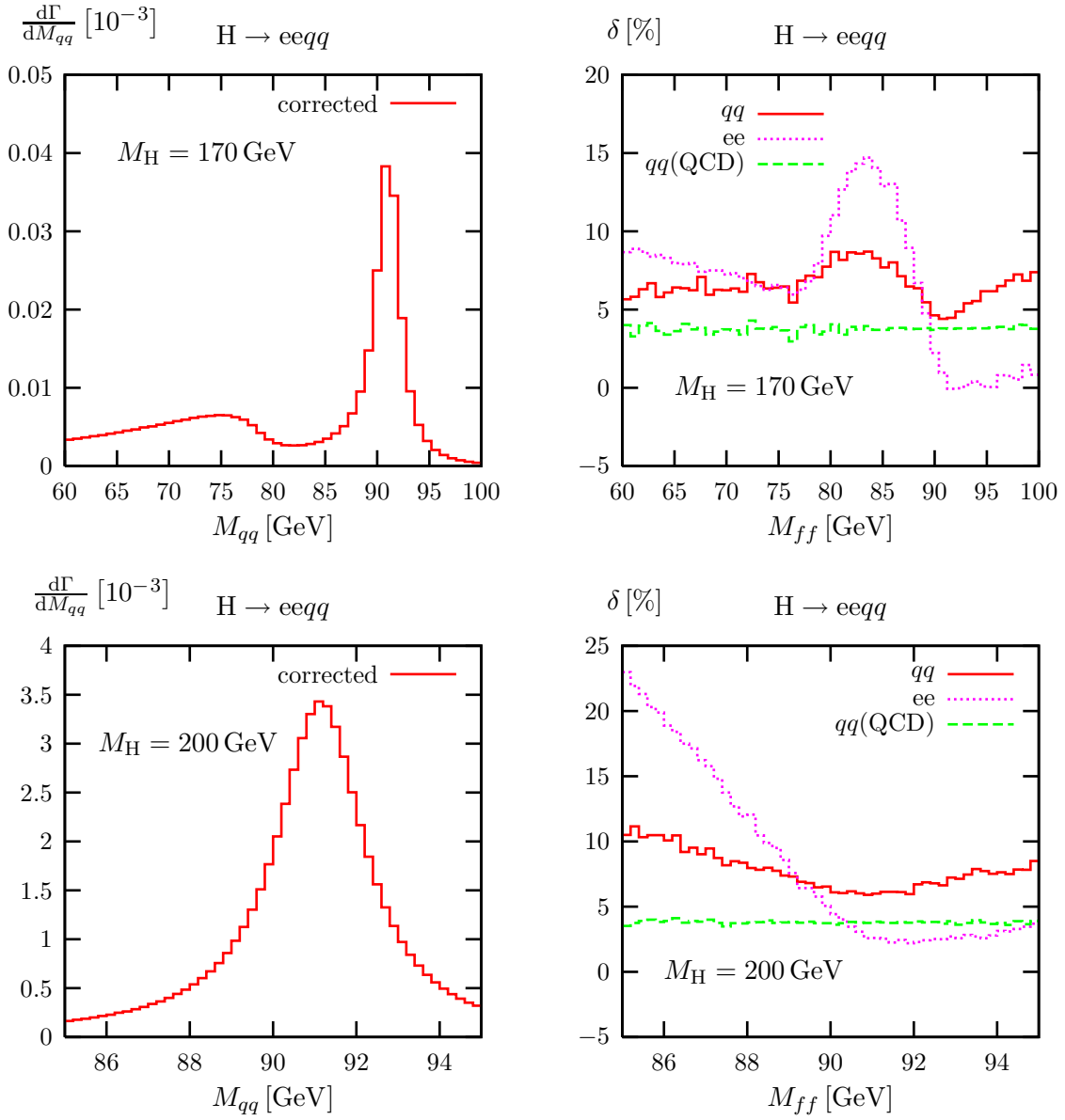


Figure 9: Distribution in the invariant mass of the  $qq$  pair (l.h.s.) and relative EW+QCD corrections to the distributions in the invariant mass of the  $ee$  and  $qq$  pairs (r.h.s) in the decay  $H \rightarrow eeqq$  for  $M_H = 170$  GeV and  $M_H = 200$  GeV. For the distribution in  $M_{qq}$  the relative QCD corrections are separately shown.

would be much larger because of mass-singular corrections proportional to  $\alpha \ln(m_l/M_H)$ , as discussed in Ref. [12].

In Figure 10 we show the distribution in the invariant mass of the  $qq$  pair and relative corrections to the distributions in the invariant mass of the  $e\nu$  and  $qq$  pairs in the decay  $H \rightarrow e\nu qq$  for  $M_H = 140$  GeV and  $M_H = 170$  GeV. Similarly to the decay  $H \rightarrow eeqq$  there is a resonance around the W-boson mass and, for  $M_H < 2M_W$ , an additional enhancement for  $M_{qq} < M_H - M_W \approx 60$  GeV where the  $e\nu$  pair can become resonant. Also the relative corrections show the same characteristics. The corrections for the  $M_{e\nu}$  distribution are somewhat smaller than for the  $M_{ee}$  distribution in Figure 9, since the neutrino does not radiate photons.

#### 4.4 Angular distributions

Angular distributions can be used to discriminate the Higgs-boson signal from the background or to study the properties of the Higgs boson. In Figure 11 we show the distribution in the angle between the decay planes of the reconstructed Z bosons in the decay  $H \rightarrow eeqq$  in the rest frame of the Higgs boson. This angle can, for instance, be used to determine the parity of the Higgs boson [11]. Since the two jets cannot be distinguished, we show the distribution in the variable

$$|\cos \phi| = \frac{|(\mathbf{k}_{\text{had}} \times \mathbf{k}_1)(\mathbf{k}_{\text{jet1}} \times \mathbf{k}_{\text{jet2}})|}{|\mathbf{k}_{\text{had}} \times \mathbf{k}_1| |\mathbf{k}_{\text{jet1}} \times \mathbf{k}_{\text{jet2}}|}, \quad (4.2)$$

which is symmetric with respect to the interchange of the jet momenta  $\mathbf{k}_{\text{jet1}}$  and  $\mathbf{k}_{\text{jet2}}$ . Here the total hadronic momentum  $\mathbf{k}_{\text{had}}$  is equal to the sum of the two jet momenta,  $\mathbf{k}_{\text{jet1}} + \mathbf{k}_{\text{jet2}}$ , because we enforce 2-jet events, and  $\mathbf{k}_1$  is the momentum of the electron. For  $M_H = 200$  GeV, both QCD and EW corrections are positive and about 4%. For  $M_H = 170$  GeV, the EW corrections are only about 2%. Both the EW and QCD corrections to this distribution are flat, in contrast to the EW corrections to the distribution in  $\cos \phi^{(\prime)}$  shown in Ref. [12] for analogous definitions of angles  $\phi^{(\prime)}$  between the two planes defined by leptonically decaying Z bosons. This difference results from the fact that the sign of  $\cos \phi^{(\prime)}$  is only observable in the purely leptonic case.

In the decay  $H \rightarrow e\nu qq$ , angles between the electron and jets can be used for background reduction [8]. In Figure 12 we show the distribution in the angle between the electron and the W boson that is reconstructed from the  $qq$  pair in the rest frame of the Higgs boson and the corresponding relative QCD and EW corrections. The plot shows the well-known property that the electron is predominantly produced in the direction opposite to the hadronically decaying W boson. The QCD corrections are about 4% and the EW corrections at the level of 5%. The complete corrections can reach up to 12% depending on the value of the Higgs-boson mass. Since the EW corrections depend on the angle they distort the distribution by a few per cent.

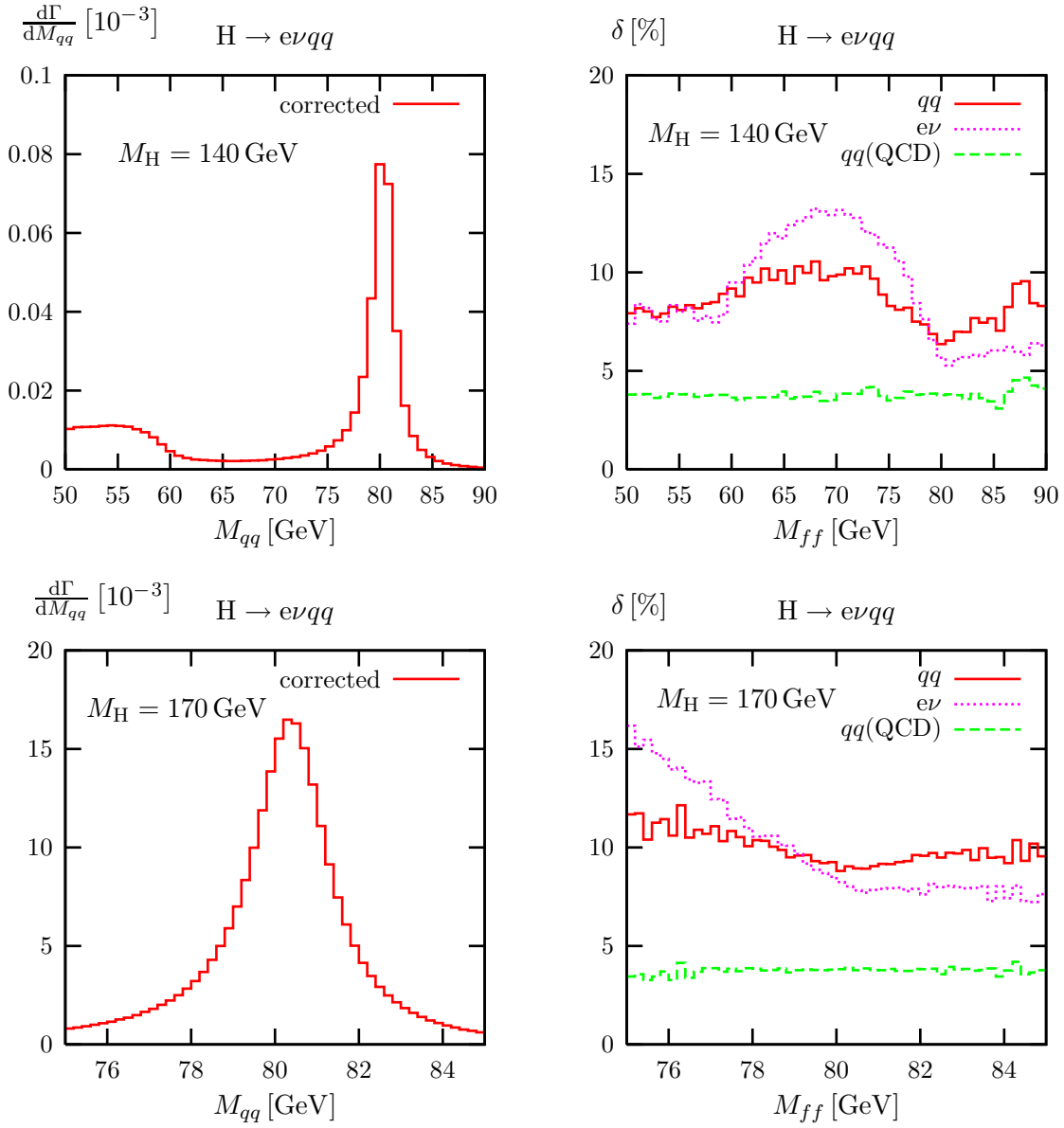


Figure 10: Distribution in the invariant mass of the  $qq$  pair (l.h.s.) and relative EW+QCD corrections to the distributions in the invariant mass of the  $e\nu$  and  $qq$  pairs (r.h.s) in the decay  $H \rightarrow e\nu qq$  for  $M_H = 140$  GeV and  $M_H = 170$  GeV. For the distribution in  $M_{qq}$  the relative QCD corrections are separately shown.

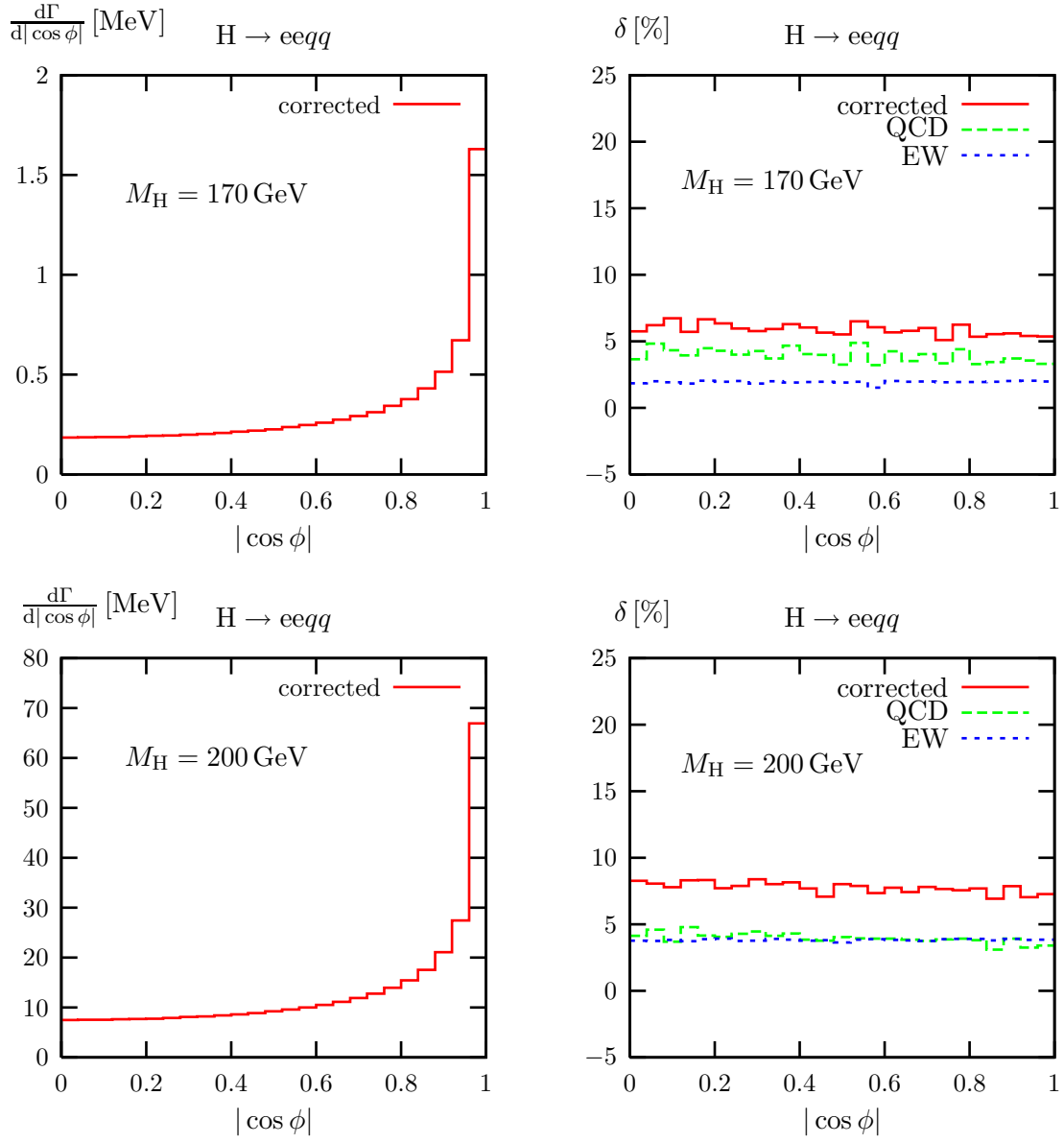


Figure 11: Distribution in the angle between the  $Z \rightarrow ee$  and  $Z \rightarrow qq$  decay planes in the decay  $H \rightarrow eeqq$  (l.h.s.) and corresponding relative EW and QCD corrections (r.h.s.) for  $M_H = 170$  GeV and  $M_H = 200$  GeV.

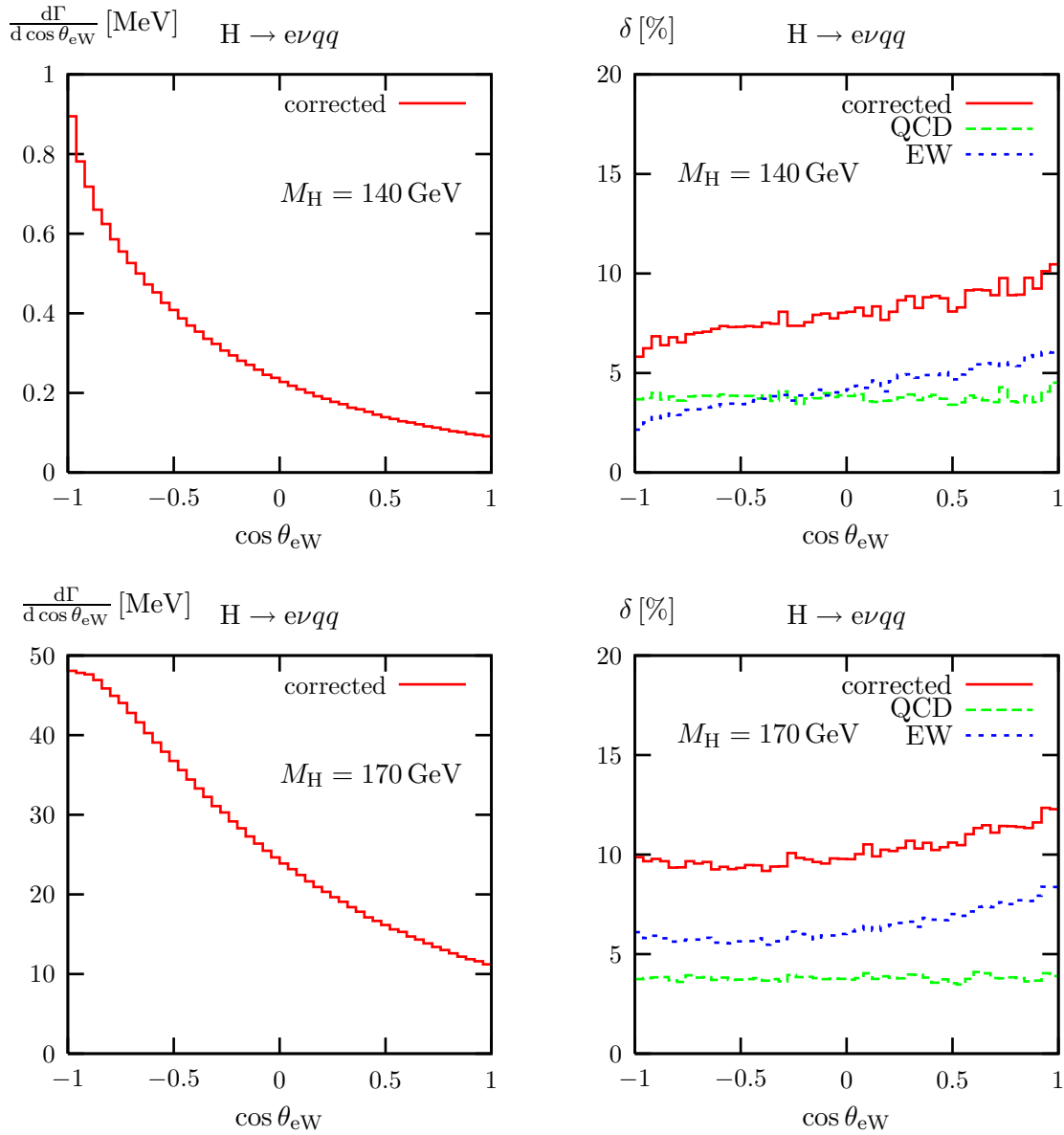


Figure 12: Distribution in the angle between the electron and the W boson reconstructed from the  $qq$  pair (l.h.s.) and corresponding relative EW and QCD corrections (r.h.s.) in the decay  $H \rightarrow e\nu qq$  for  $M_H = 140$  GeV and  $M_H = 170$  GeV.



## 5 Conclusions

The decays of the Standard Model Higgs boson into four fermions via a W-boson or Z-boson pair lead to experimental signatures at the LHC and at a future  $e^+e^-$  linear collider that are both important for the search for the Higgs boson and for studying its properties. In order to allow for adequate theoretical predictions for these decays, a Monte Carlo event generator is needed that properly accounts for the relevant radiative corrections. PROPHECY4F is such an event generator which provides accurate predictions above, in the vicinity of, and below the WW and ZZ thresholds, owing to the use of the complex-mass scheme for the treatment of the gauge-boson resonances.

While PROPHECY4F originally contained only the electroweak corrections, in this paper we have included also the complete  $\mathcal{O}(\alpha_s)$  QCD corrections. This allows to study precise predictions for all leptonic, semileptonic, and hadronic final states.

The QCD corrections to the partial decay widths are dominated by the corrections to the gauge-boson decays and roughly given by  $\alpha_s/\pi \approx 3.8\%$  for semileptonic and  $2\alpha_s/\pi \approx 7.6\%$  for hadronic final states. The electroweak corrections to the partial decay widths are very similar for leptonic, hadronic, and semileptonic final states. They are positive, typically amount to some per cent, increase with growing Higgs mass  $M_H$ , and reach about 8% at  $M_H \sim 500$  GeV. In the on-shell (narrow-width) approximation for the intermediate gauge bosons, the correction is good within 1–2% of the partial widths for Higgs-boson masses sufficiently above the corresponding gauge-boson pair threshold, as long as the lowest-order prediction consistently includes the off-shell effects of the gauge bosons. For  $H \rightarrow WW \rightarrow 4f$  the narrow-width approximation fails badly close to the WW threshold, because the instability of the W bosons significantly influences the Coulomb singularity near threshold. Only a calculation that keeps the full off-shellness of the W and Z bosons can describe the threshold regions properly. A simple improved Born approximation for the partial widths reproduces the full calculation within  $\lesssim 2\text{--}3\%$  for Higgs-boson masses below 400 GeV. In this regime our complete calculation should have a theoretical uncertainty below 1%. For larger Higgs-boson masses we expect that unknown two-loop corrections that are enhanced by  $G_\mu M_H^2$  deteriorate the accuracy. Finally, for  $M_H \gtrsim 700$  GeV it is well known that perturbative predictions become questionable in general.

We have numerically investigated distributions for semileptonic final states where collinear photons are recombined and 2-jet events are forced. For angular and invariant-mass distributions the QCD corrections are flat and reflect the corresponding corrections to the integrated decay widths. For angular distributions, which can be used for background reduction or the study of the quantum numbers of the Higgs boson, the electroweak corrections are of the order of 5–10% and, in general, distort the shapes. For invariant-mass distributions of fermion pairs, which are relevant for the reconstruction of the gauge bosons, well-known large photonic corrections show up and can exceed 10% depending on the treatment of photon radiation.

This work completes the physics part of the Monte Carlo event generator PROPHECY4F for  $H \rightarrow WW/ZZ \rightarrow 4f$ . It now includes the complete  $\mathcal{O}(\alpha)$  electroweak and  $\mathcal{O}(\alpha_s)$  QCD corrections as well as corrections beyond  $\mathcal{O}(\alpha)$  originating from heavy-Higgs effects and final-state photon radiation for all possible 4-fermion final states. PROPHECY4F works

at the parton level and generates weighted events; unweighted event generation and an interface to parton showering will be addressed in the future.

## Acknowledgements

A.B. was supported by a fellowship within the Postdoc programme of the German Academic Exchange Service (DAAD).

## References

- [1] E. W. N. Glover, J. Ohnemus and S. S. D. Willenbrock, *Phys. Rev. D* **37** (1988) 3193;  
V. D. Barger, G. Bhattacharya, T. Han and B. A. Kniehl, *Phys. Rev. D* **43** (1991) 779;  
V. D. Barger, R. J. N. Phillips and D. Zeppenfeld, *Phys. Lett. B* **346** (1995) 106 [hep-ph/9412276];  
M. Dittmar and H. K. Dreiner, *Phys. Rev. D* **55** (1997) 167 [hep-ph/9608317];  
D. L. Rainwater and D. Zeppenfeld, *Phys. Rev. D* **60** (1999) 113004 [Erratum-ibid. *D* **61** (2000) 099901] [hep-ph/9906218];  
N. Kauer, T. Plehn, D. L. Rainwater and D. Zeppenfeld, *Phys. Lett. B* **503** (2001) 113 [hep-ph/0012351].
- [2] S. Asai *et al.*, *Eur. Phys. J. C* **32S2** (2004) 19 [hep-ph/0402254];  
S. Abdullin *et al.*, *Eur. Phys. J. C* **39S2** (2005) 41.
- [3] L. Zivkovic, *Czech. J. Phys.* **54** (2004) A73.
- [4] ATLAS Collaboration, Technical Design Report, vol. II, CERN–LHCC 99-15 (May 1999).
- [5] CMS Collaboration, Technical Design Report v.2 : Physics performance, Technical Proposal, CERN-LHCC-2006-021 (2006);  
K. A. Assamagan *et al.* [Higgs Working Group Collaboration], proceedings of the 3rd Les Houches Workshop: “Physics at TeV Colliders”, Les Houches, 2003, hep-ph/0406152;  
C. Buttar *et al.* [SMH Working Group Collaboration] QCD, EW, and Higgs working group report of the workshop “Physics at TeV Colliders”, Les Houches, May 2005, hep-ph/0604120.
- [6] J. A. Aguilar-Saavedra *et al.*, TESLA Technical Design Report Part III: Physics at an  $e^+e^-$  Linear Collider, hep-ph/0106315;  
T. Abe *et al.* [American Linear Collider Working Group Collaboration], in *Proc. of the APS/DPF/DPB Summer Study on the Future of Particle Physics (Snowmass 2001)* ed. R. Davidson and C. Quigg, SLAC-R-570, *Resource book for Snowmass 2001*, [hep-ex/0106055, hep-ex/0106056, hep-ex/0106057, hep-ex/0106058];  
K. Abe *et al.* [ACFA Linear Collider Working Group Collaboration], ACFA Linear Collider Working Group report, [hep-ph/0109166].

- [7] N. Meyer and K. Desch, *Eur. Phys. J. C* **35** (2004) 171.
- [8] V. Cavasinni, D. Constanzo, E. Mazzone and I. Vivarelli, ATLAS note ATL-PHYS-2002-110.
- [9] H. Pi, P. Avery, J. Rohlf, C. Tulli and S. Kunori, CMS note 2006/092 (2006).
- [10] P. Garcia-Abia, W. Lohmann and A. Raspereza, *Eur. Phys. J. C* **44** (2005) 481.
- [11] C. A. Nelson, *Phys. Rev. D* **37** (1988) 1220;  
A. Soni and R. M. Xu, *Phys. Rev. D* **48** (1993) 5259 [hep-ph/9301225];  
D. Chang, W. Y. Keung and I. Phillips, *Phys. Rev. D* **48** (1993) 3225 [hep-ph/9303226];  
A. Skjold and P. Osland, *Phys. Lett. B* **311** (1993) 261 [hep-ph/9303294];  
V.D. Barger, K.M. Cheung, A. Djouadi, B.A. Kniehl and P.M. Zerwas, *Phys. Rev. D* **49** (1994) 79 [hep-ph/9306270];  
T. Arens and L. M. Sehgal, *Z. Phys. C* **66** (1995) 89 [hep-ph/9409396];  
C. P. Buszello, I. Fleck, P. Marquard and J. J. van der Bij, *Eur. Phys. J. C* **32** (2004) 209 [hep-ph/0212396];  
S. Y. Choi, D. J. Miller, M. M. Mühlleitner and P. M. Zerwas, *Phys. Lett. B* **553** (2003) 61 [hep-ph/0210077].
- [12] A. Bredenstein, A. Denner, S. Dittmaier and M. M. Weber, *Phys. Rev. D* **74** (2006) 013004 [hep-ph/0604011].
- [13] A. Djouadi, hep-ph/0503172.
- [14] J. Fleischer and F. Jegerlehner, *Phys. Rev. D* **23** (1981) 2001;  
B.A. Kniehl, *Nucl. Phys. B* **352** (1991) 1;  
D.Y. Bardin, P.K. Khristova and B.M. Vilensky, *Sov. J. Nucl. Phys.* **54** (1991) 833 [*Yad. Fiz.* **54** (1991) 1366];  
B.A. Kniehl, *Nucl. Phys. B* **357** (1991) 439.
- [15] B. A. Kniehl and M. Spira, *Z. Phys. C* **69** (1995) 77 [hep-ph/9505225];  
B. A. Kniehl and M. Steinhauser, *Phys. Lett. B* **365** (1996) 297 [hep-ph/9507382];  
B. A. Kniehl and M. Steinhauser, *Nucl. Phys. B* **454** (1995) 485 [hep-ph/9508241];  
A. Djouadi, P. Gambino and B. A. Kniehl, *Nucl. Phys. B* **523** (1998) 17 [hep-ph/9712330].
- [16] A. Ghinculov, *Nucl. Phys. B* **455** (1995) 21 [hep-ph/9507240];  
A. Frink, B.A. Kniehl, D. Kreimer and K. Riesselmann, *Phys. Rev. D* **54** (1996) 4548 [hep-ph/9606310].
- [17] A. Bredenstein, A. Denner, S. Dittmaier and M. M. Weber, *Nucl. Phys. Proc. Suppl.* **160** (2006) 131 [hep-ph/0607060].
- [18] C. M. Carloni Calame, M. Moretti, G. Montagna, O. Nicrosini, F. Piccinini and A. D. Polosa, *Nucl. Phys. Proc. Suppl.* **157** (2006) 73 [hep-ph/0604033].

- [19] A. Denner, Fortsch. Phys. **41** (1993) 307.
- [20] A. Denner, G. Weiglein and S. Dittmaier, Nucl. Phys. B **440** (1995) 95 [hep-ph/9410338].
- [21] A. Denner, S. Dittmaier, M. Roth and D. Wackerroth, Nucl. Phys. B **560** (1999) 33 [hep-ph/9904472]; Comput. Phys. Commun. **153** (2003) 462 [hep-ph/0209330].
- [22] A. Denner, S. Dittmaier, M. Roth and L. H. Wieders, Nucl. Phys. B **724** (2005) 247 [hep-ph/0505042].
- [23] A. Denner and S. Dittmaier, Nucl. Phys. Proc. Suppl. **160** (2006) 22 [hep-ph/0605312].
- [24] J. Küblbeck, M. Böhm and A. Denner, Comput. Phys. Commun. **60** (1990) 165; H. Eck and J. Küblbeck, *Guide to FeynArts 1.0*, University of Würzburg, 1992.
- [25] T. Hahn, Comput. Phys. Commun. **140** (2001) 418 [hep-ph/0012260].
- [26] T. Hahn and M. Perez-Victoria, Comput. Phys. Commun. **118** (1999) 153 [hep-ph/9807565];  
T. Hahn, Nucl. Phys. Proc. Suppl. **89** (2000) 231 [hep-ph/0005029].
- [27] A. Denner, S. Dittmaier, M. Roth and M.M. Weber, Nucl. Phys. B **660** (2003) 289 [hep-ph/0302198].
- [28] A. Denner, S. Dittmaier, M. Roth and L. H. Wieders, Phys. Lett. B **612**, 223 (2005) [hep-ph/0502063].
- [29] G. 't Hooft and M. Veltman, Nucl. Phys. B **153** (1979) 365;  
W. Beenakker and A. Denner, Nucl. Phys. B **338** (1990) 349;  
A. Denner, U. Nierste and R. Scharf, Nucl. Phys. B **367** (1991) 637.
- [30] A. Denner and S. Dittmaier, Nucl. Phys. B **658** (2003) 175 [hep-ph/0212259].
- [31] G. Passarino and M. Veltman, Nucl. Phys. B **160** (1979) 151.
- [32] A. Denner and S. Dittmaier, Nucl. Phys. B **734** (2006) 62 [hep-ph/0509141].
- [33] S. Dittmaier, Phys. Rev. D **59** (1999) 016007 [hep-ph/9805445].
- [34] T. Stelzer and W.F. Long, Comput. Phys. Commun. **81** (1994) 357 [hep-ph/9401258].
- [35] S. Dittmaier, Nucl. Phys. B **565** (2000) 69 [hep-ph/9904440].
- [36] M. Böhm and S. Dittmaier, Nucl. Phys. B **409** (1993) 3 and Nucl. Phys. B **412** (1994) 39;  
U. Baur, S. Keller and D. Wackerroth, Phys. Rev. D **59** (1999) 013002 [hep-ph/9807417].
- [37] A. Bredenstein, S. Dittmaier and M. Roth, Eur. Phys. J. C **44** (2005) 27 [hep-ph/0506005].

- [38] W. Beenakker *et al.*, in *Physics at LEP2*, eds. G. Altarelli, T. Sjöstrand and F. Zwirner (CERN 96-01, Geneva, 1996), Vol. 1, p. 79 [hep-ph/9602351].
- [39] F. A. Berends, R. Pittau and R. Kleiss, Nucl. Phys. B **424** (1994) 308 [hep-ph/9404313] and Comput. Phys. Commun. **85** (1995) 437 [hep-ph/9409326];  
F. A. Berends, P. H. Daverveldt and R. Kleiss, Nucl. Phys. B **253** (1985) 441;  
J. Hilgart, R. Kleiss and F. Le Diberder, Comput. Phys. Commun. **75** (1993) 191.
- [40] A. Bredenstein, S. Dittmaier and M. Roth, Eur. Phys. J. C **36** (2004) 341 [hep-ph/0405169].
- [41] G.P. Lepage, J. Comput. Phys. **27** (1978) 192.
- [42] R. K. Ellis, W. T. Giele and G. Zanderighi, Phys. Rev. D **72** (2005) 054018 [Erratum-  
ibid. D **74** (2006) 079902] [hep-ph/0506196].